A Parametric Study of Spur Gear Dynamics

Hsiang Hsi Lin and Chuen-Huei Liou
The University of Memphis, Memphis, Tennessee

19980209 148

Since its founding, NASA has been dedicated to the advancement of aeronautics and space science. The NASA Scientific and Technical Information (STI) Program Office plays a key part in helping NASA maintain this important role.

The NASA STI Program Office is operated by Langley Research Center, the Lead Center for NASA's scientific and technical information. The NASA STI Program Office provides access to the NASA STI Database, the largest collection of aeronautical and space science STI in the world. The Program Office is also NASA's institutional mechanism for disseminating the results of its research and development activities. These results are published by NASA in the NASA STI Report Series, which includes the following report types:

- TECHNICAL PUBLICATION. Reports of completed research or a major significant phase of research that present the results of NASA programs and include extensive data or theoretical analysis. Includes compilations of significant scientific and technical data and information deemed to be of continuing reference value. NASA's counterpart of peer-reviewed formal professional papers but has less stringent limitations on manuscript length and extent of graphic presentations.

- TECHNICAL MEMORANDUM. Scientific and technical findings that are preliminary or of specialized interest, e.g., quick release reports, working papers, and bibliographies that contain minimal annotation. Does not contain extensive analysis.

- CONTRACTOR REPORT. Scientific and technical findings by NASA-sponsored contractors and grantees.

- CONFERENCE PUBLICATION. Collected papers from scientific and technical conferences, symposia, seminars, or other meetings sponsored or cosponsored by NASA.

- SPECIAL PUBLICATION. Scientific, technical, or historical information from NASA programs, projects, and missions, often concerned with subjects having substantial public interest.

- TECHNICAL TRANSLATION. English-language translations of foreign scientific and technical material pertinent to NASA's mission.

Specialized services that complement the STI Program Office's diverse offerings include creating custom thesauri, building customized data bases, organizing and publishing research results . . . even providing videos.

For more information about the NASA STI Program Office, see the following:

- Access the NASA STI Program Home Page at *http://www.sti.nasa.gov*

- E-mail your question via the Internet to help@sti.nasa.gov

- Fax your question to the NASA Access Help Desk at (301) 621-0134

- Telephone the NASA Access Help Desk at (301) 621-0390

- Write to:
  NASA Access Help Desk
  NASA Center for AeroSpace Information
  800 Elkridge Landing Road
  Linthicum Heights, MD 21090-2934

Available from

A PARAMETRIC STUDY OF SPUR GEAR DYNAMICS

Hsiang Hsi Lin and Chuen-Huei Liou
Department of Mechanical Engineering
The University of Memphis
Memphis, Tennessee

ABSTRACT

A parametric study of a spur gear system was performed through a numerical analysis approach. This study used the gear dynamic program DANST, a computer simulator, to determine the dynamic behavior of a spur gear system. The analytical results have taken the deflection of shafts and bearings into consideration for static analysis, and the influence of these deflections on gear dynamics was investigated.

Damping in the gear system usually is an unknown quantity, but it has an important effect in resonance vibration. Typical values as reported in the literature were used in the present analysis. The dynamic response due to different damping factors was evaluated and compared.

The effect of the contact ratio on spur gear dynamic load and dynamic stress was investigated through a parameter study. The contact ratio was varied over the range of 1.26 to 2.46 by adjusting the tooth addendum. Gears with contact ratio near 2.0 were found to have the most favorable dynamic performance.

CHAPTER I

INTRODUCTION

Power transfer is necessary from source to application in mechanical power systems. Compared with other transmission members, gears have several advantages considering their small overall dimensions, constant transmission ratio and operating simplicity. Therefore, they have the widest application in mechanical engineering for transmission of power. The art and science of gear transmission systems continue to improve. Today's engineers and researchers delve into many areas of innovative advancement and seek to establish and modify methods which can make gear systems meet the ever-widening needs of advancing technology. Their objectives are improvements of transmission life, operating efficiency, and reliability. They also seek to increase the power-to-weight ratio and to reduce noise and vibration of gear transmissions.

Research on gear noise and vibration has revealed that the basic mechanism of noise generated from gearing is vibration excited by the dynamic load. Dynamic load carrying behavior of gears is strongly influenced by geometric deviations associated with manufacturing, assembly and deformation processes. High dynamic load can lead to fatigue failure and affect the life and reliability of a gear transmission. Minimizing gear dynamic load will decrease gear noise, increase efficiency, improve pitting fatigue life, and help prevent gear tooth fracture. At present, concerted gear transmission system studies have been concentrated on two main effects. These studies have been on: (1) The localized tooth stress effects during gear interactions, and (2) the overall global dynamic behavior of the systems.

The problem of dynamic loads acting on gear teeth was first studied in the early 1930's by the ASME Research Committee and tests were conducted by Lewis and Buckingham [1]. Their report indicated a procedure to determine the dynamic load increment due to dynamics of gears

1

in mesh and the error of the gear teeth. Tuplin [2] was one of the first to publish a more refined method of determining the dynamic load in gear teeth. He considered gear meshing as an equivalent spring-mass model with constant stiffness subjected to wedge or sinusoidal excitations. Cloutier [3], Gregory [4], etc. later modified this model by introducing spring as a time varying stiffness. In 1977, Cornell and Westervelt [5] developed a time history, closed form solution of a dynamic model of spur gear system which consisted of a cantilever beam with a cam moving along it for simulating the engagement and disengagement of the adjacent tooth to generate the dynamic load for meshing teeth. This dynamic model was based on Richardson's cam model [6], but treated the teeth as a variable spring. They stated that the nonlinearity of the tooth pair stiffness during mesh, the tooth error, and the profile modifications had significant effects upon the dynamic load. The studies on geared rotor dynamics have been rather recent. Several modeling and solution techniques such as lumped mass models and the use of the transfer matrix method and finite element method have been applied to rotor dynamics problems. Hamad and Seireg [7] studied the whirling of geared rotor systems without considering torsional vibrations and the gear shaft was assumed to be rigid. Iida, et al. [8] considered the same problem by taking one of the shafts to be rigid and neglecting the compliance of the gear mesh. He obtained a three degree of freedom model to determine the response of the first three vibration modes. In 1984, Iwatsubo, Arii and Kawai [9] used the transfer matrix method to evaluate the forced response due only to the mass unbalance in the rotor system. Later, they [10] included the effects of periodic variation of mesh stiffness and profile errors of both gears. Since computer usage has become popular in the 80's and 90's. Tedious computation now can be easily done through computer modeling by writing appropriate code. Finite element methods are widely used in engineering analysis. Ozguren and Houser [11,12] used a spatial finite line-element technique to perform mode shape and frequency analysis in geared rotor systems. Also,

2

their study included the effect of bearing flexibility which is usually neglected in simple gear dynamics models.

All of the above literature analyzed the dynamics of a gear transmission system in different aspects. Their models treated either the shaft and bearing of gear system or the gear teeth as rigid bodies depending on the purpose of analysis. In reality, none of the above components are rigid when subjected to a force. To evaluate the gear dynamic behavior more accurately, the deflections of shafts and bearings, and the deformations of gears, due to transmitted load should be taken into account in modeling the gear transmission system. The computer code DANST which was developed for the dynamic analysis of low-contact-ratio gears [13] and high-contact-ratio gears [14] was modified to conduct this study. The dynamic response of a spur gear pair is depicted by the dynamic load and stress factors. Two different gear-shaft assembly types were considered in the study. Several gear parameters such as damping and contact ratio are examined in a wide range of variation to determine their influence on gear dynamics. The computer simulation results revealed the effect of each individual parameter and can help the gear designer choose the optimum value of gear parameters when designing a gear train system for minimum dynamic load and stress.

CHAPTER II

SYSTEM CHARACTERISTICS

II.1 System Configuration

Gears are used to transmit power and/or angular motion between shafts. There exists a wide variety of types of gears with each serving a range of functions. For our investigation a simple spur gear system was used and its model is illustrated in Figure II.1, in which several basic elements such as flexible shaft, rolling element bearing, motor, and load are shown. The static properties of the components of the system were obtained from the literature of gearing, mechanics of materials, lubrication, rolling bearing, vibration, and finite element methods. They will be introduced later into dynamic investigations.

A set of governing equations of motion can be determined from the system properties, such as stiffnesses, inertias, damping factors, frictions, ... etc. The equations are then integrated and solved by a numerical method through the aid of a computer. Those solutions are based on the following assumptions: (1) the dynamic process is defined in rotating plane of the gears, (2) the torsional stiffness of the shafts and gears in engagement, and their masses are also acting in the same plane, and (3) the axes of rotation are symmetrical, and out-of-plane twisting and misalignment effects are not considered. A parametric study was performed to examine the system dynamic behavior and to evaluate and determine the best parameter values based upon the result of the simulation.

II.2 Basic Geometry of Spur Gear
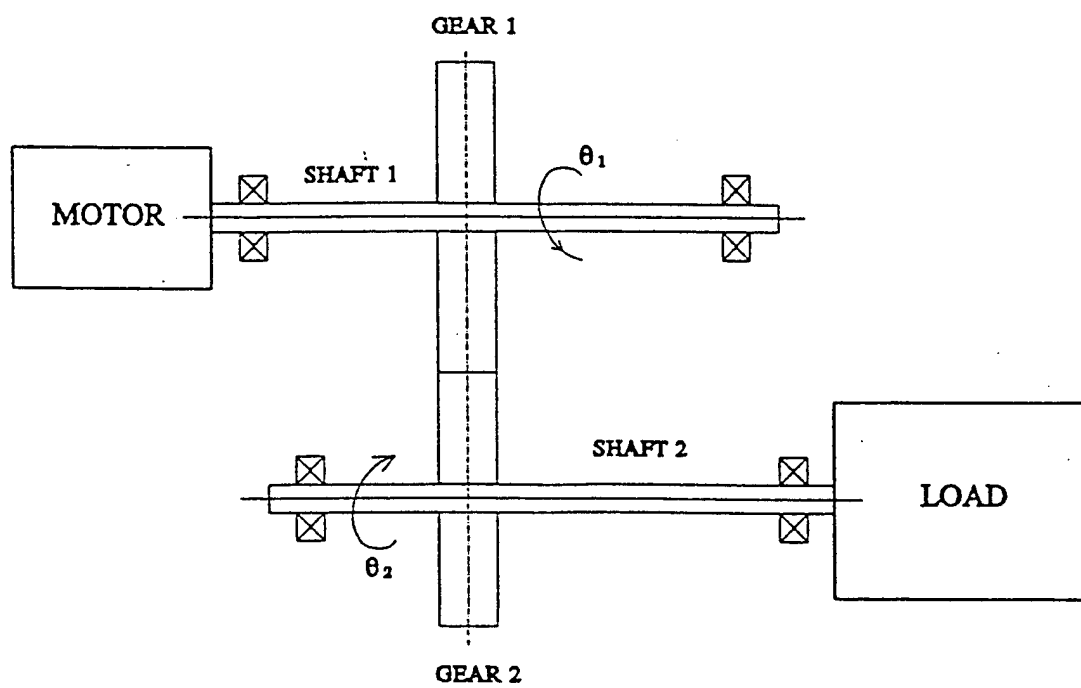
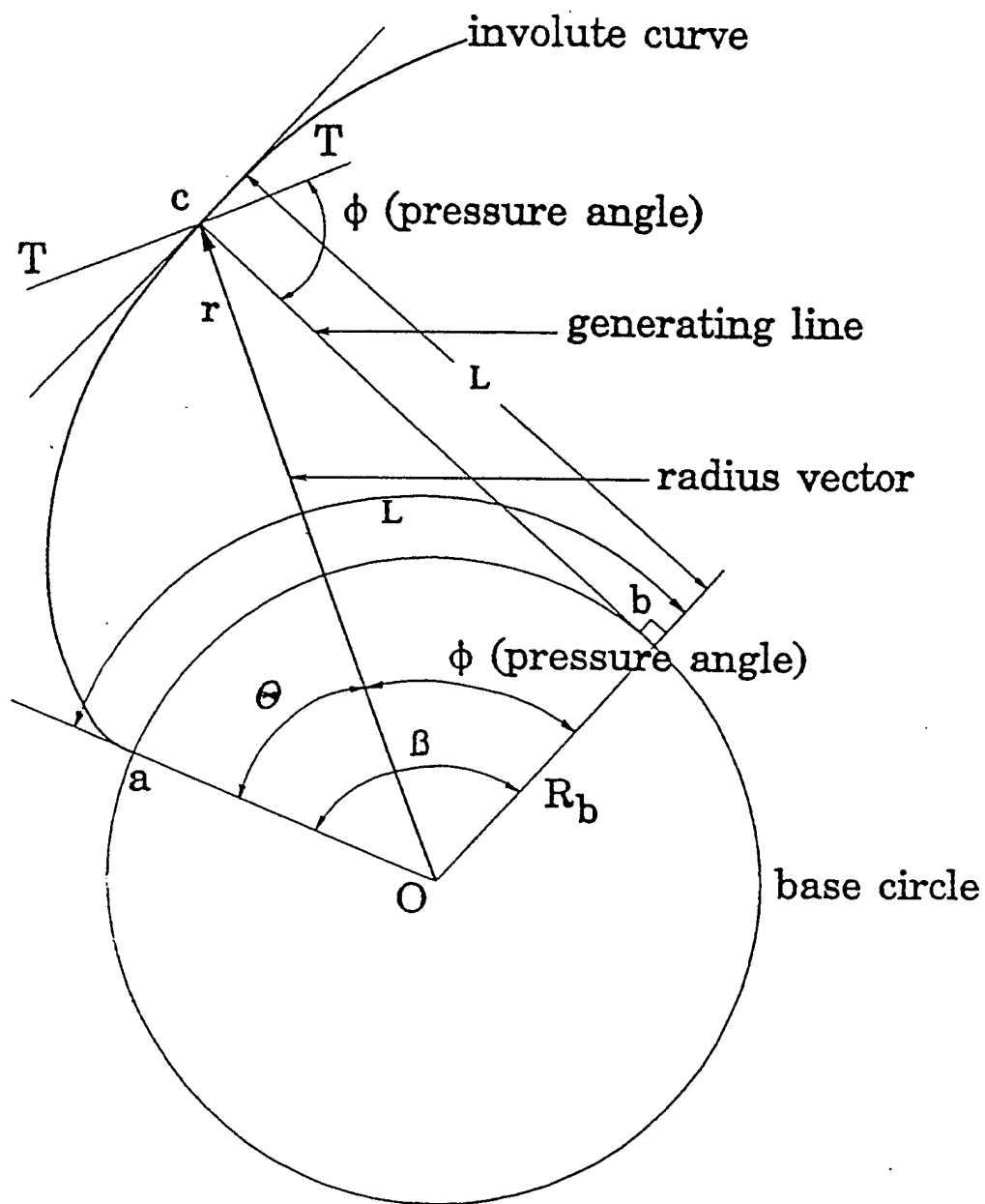### II.2.1 Involute Curve

Figure II.1 A simple spur gear system

Figure II.2 Geometry of an involute curve

For a spur gear the teeth lie parallel to the axis of rotation and are of involute form in most case. The analytical geometry of an involute curve, shown in Figure II.2, defined as the locus of any fixed point on a tangent line as this line rolls, without slipping around a circle. This process may be visualized as unwinding a string from a circular disk. The circle from which the string is unwound is called the <u>base circle</u>. The length of the generating line "L" as it lies between the involute curve at point c and point b, at which it is tangent to the base circle, is the same as its length as it was when wrapped around the base circle from point b to point a. Therefore, the geometrical relationship of the involute curve can be expressed as follows:

$$\theta = \beta - \phi = \beta - \tan^{-1}\left(\frac{\sqrt{r^2 - R_b^2}}{R_b}\right) \tag{II.1}$$

$$\sqrt{r^2 - R_b^2} = R_b\beta \tag{II.2}$$

$$\beta = \frac{\sqrt{r^2 - R_b^2}}{R_b} \tag{II.3}$$

where

R_b : radius of base circle

r : radius to any point of involute

β : angle through which line has been unwound

hence

$$\theta = \frac{\sqrt{r^2 - R_b^2}}{R_b} - \tan^{-1}\left(\frac{\sqrt{r^2 - R_b^2}}{R_b}\right) \tag{II.4}$$

This is the polar equation of the involute curve. The tangent to the involute at any point is perpendicular to the generating line and the shape of the involute is dependent only on the diameter of the base circle.

II.2.2 Contacting Involute Curve

Consider the action of two involute gear teeth transmitting angular motion by means of shafts as shown in Figure II.3. The line (AB) is called the Line of Action and it is a line tangent to the two base circles at point A and point B. If point C moves along involute is revolved at a uniform rate of motion, it changes the length of generating line (AE) uniformly. Meanwhile, the length of the generating line (BE) on the mating involute changes at the same uniform rate, because the total length of the common tangent (AB) of the two base circles remains constant. Thus, all contact between two involutes takes place along the line of action. The relative rate of motion depends only upon the relative sizes of two base circles while the relative rates of rotation are independent of the distance between the center of the two base circles.

II.2.3 Rolling and Sliding Velocity

Pure rolling occurs if two friction disks rotate in contact without slipping. However, for the case of two involute gear teeth meshing with each other, the meshing action is a combination of rolling and sliding. Figure II.4 shows two gears with equal size base circles which mesh with each other. The teeth are in contact at the pitch point P. Radii of curvature of the two involutes are shown at equal angular intervals on each base circle. The arc XY which describes the tooth profile on gear I and the arc AB which describes the tooth profile on gear II have different lengths. Therefore, the two profiles must slide over each other during mesh to make up the
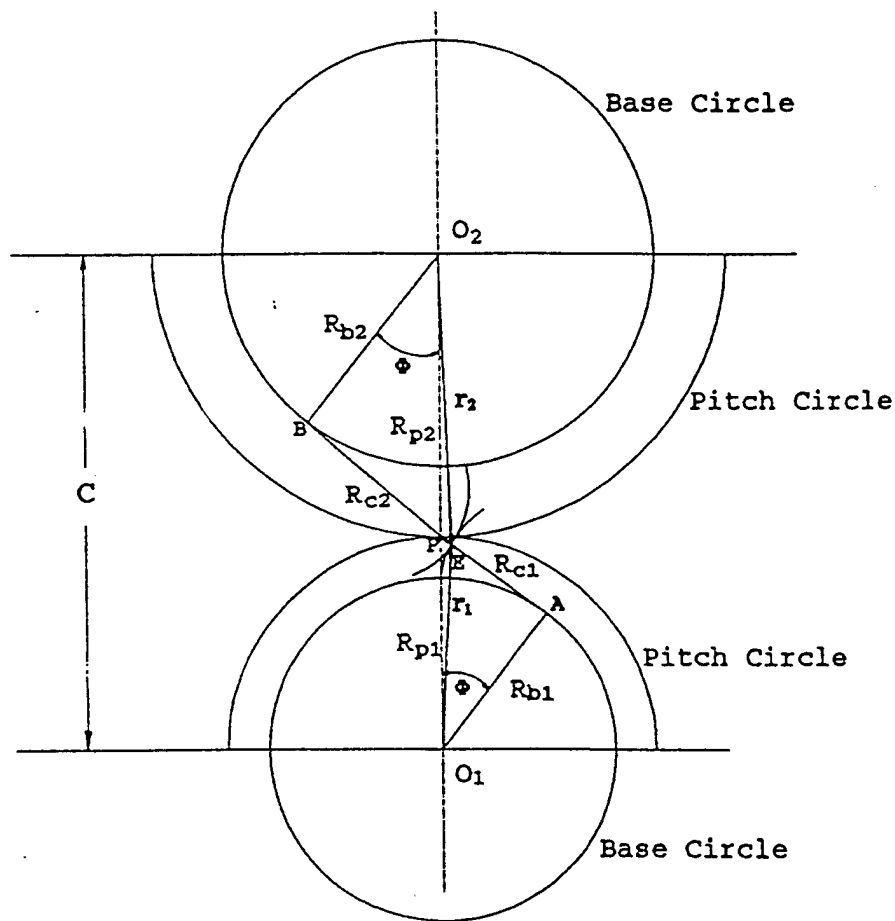
8

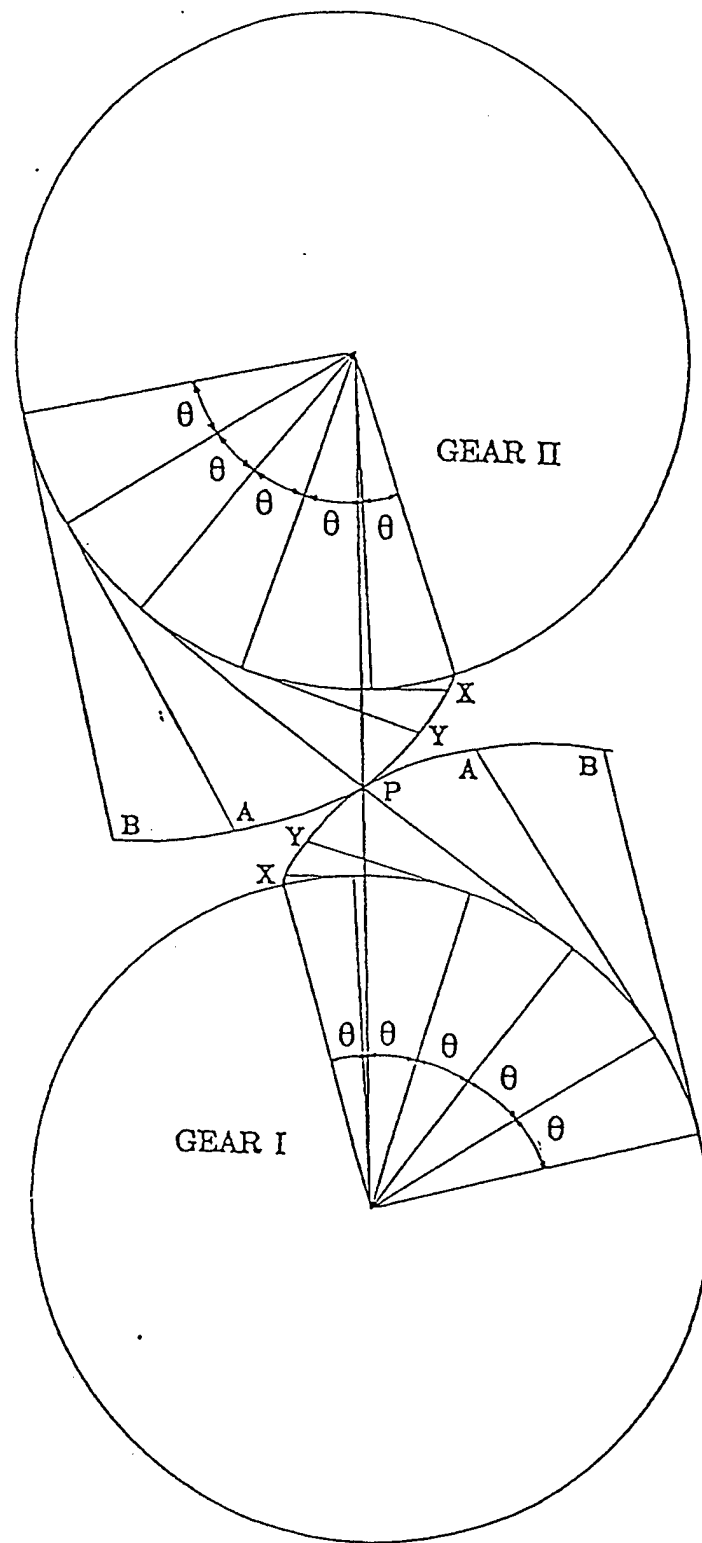Figure II.3 Meshing diagram of an involute gear pair

Figure II.4 Profile length difference between two mating involute curves

difference in the arc lengths. Under this condition, the sliding velocity at any point is calculated

as:

$$V_s = \frac{R_{C1}\ \omega_1 - R_{C2}\ \omega_2}{12} \qquad \text{(II.5)}$$

By referring to Figure II.3, the following expressions are obtained:

$$\omega_1 = \frac{12\ V}{R_{P1}} \qquad \text{(II.6)}$$

$$\omega_2 = \frac{R_{P1}\ \omega_1}{R_{P2}} \qquad \text{(II.7)}$$

$$V = \frac{2\ \pi\ R_{P1}\ n}{12} = \frac{R_{P1}\ \omega_1}{12} \qquad \text{(II.8)}$$

$$R_{C1} + R_{C2} = C \sin \phi \qquad \text{(II.9)}$$

$$R_{C1} = \sqrt{r_1^2 - R_{b1}^2} \qquad \text{(II.10)}$$

$$R_{C2} = \sqrt{r_2^2 - R_{b1}^2} = C \sin \phi - \sqrt{R_1^2 - R_{b1}^2} \qquad \text{(II.11)}$$

where

R_{p1}, R_{p2} : radius of pitch circle of gear, in

R_{b1}, R_{b2} : radius of base circle of gear, in

r_1, r_2 : any radius of gear-tooth profile, in

R_{c1}, R_{c2} : radius of curvature of gear at r_1, r_2, in

11

W_1, W_2 : angular velocity of gear, rad/min

C : center distance, in

n : speed of driving gear, rpm

V : pitch-line velocity of gears, ft/min

V_s : sliding velocity, ft/min

ϕ : pressure angle, degree

Using the above parameters, the sliding velocity equation can be rewritten as:

$$V_s = \left[\frac{V \left(R_{P1} + R_{P2} \right)}{R_{P1} \, R_{P2}} \right] \left(\sqrt{r_1^2 - R_{b1}^2} - R_{P1} \sin \phi \right) \qquad \textbf{(II.12)}$$

II.3 Elastic Deflection and Stiffness of Spur Gear Teeth

A pair of teeth in contact due to the load will deflect elastically. According to R.W. Cornell's

nonlinear compliance model [5] this deflection is based on a combination of the deflection of the

tooth as a cantilever beam, local contact compression, and fillet and tooth foundation flexibility

effects. All of the above except the local contact compression are linear functions of the load.

The nonlinear term is due to the Hertzian deflection. The total deflection of a gear tooth can be

expressed along a line normal to the tooth profile. Since the gear tooth is stubby, both the

foundation and the shear effects are essential. To calculate tooth deflection, first, it is assumed

that the involute portion of a gear tooth is a non-uniform cantilever beam with an effective length

l_0 which extends from the tooth tip to the beginning of fillet area as shown in Figure II.5,

Secondly, by dividing this section into a sequence of segments and using elementary strength of

materials theory, both deflection and compliance of this tooth portion can be calculated. The

formulas for the above-mentioned procedure are depicted in the following sections. More

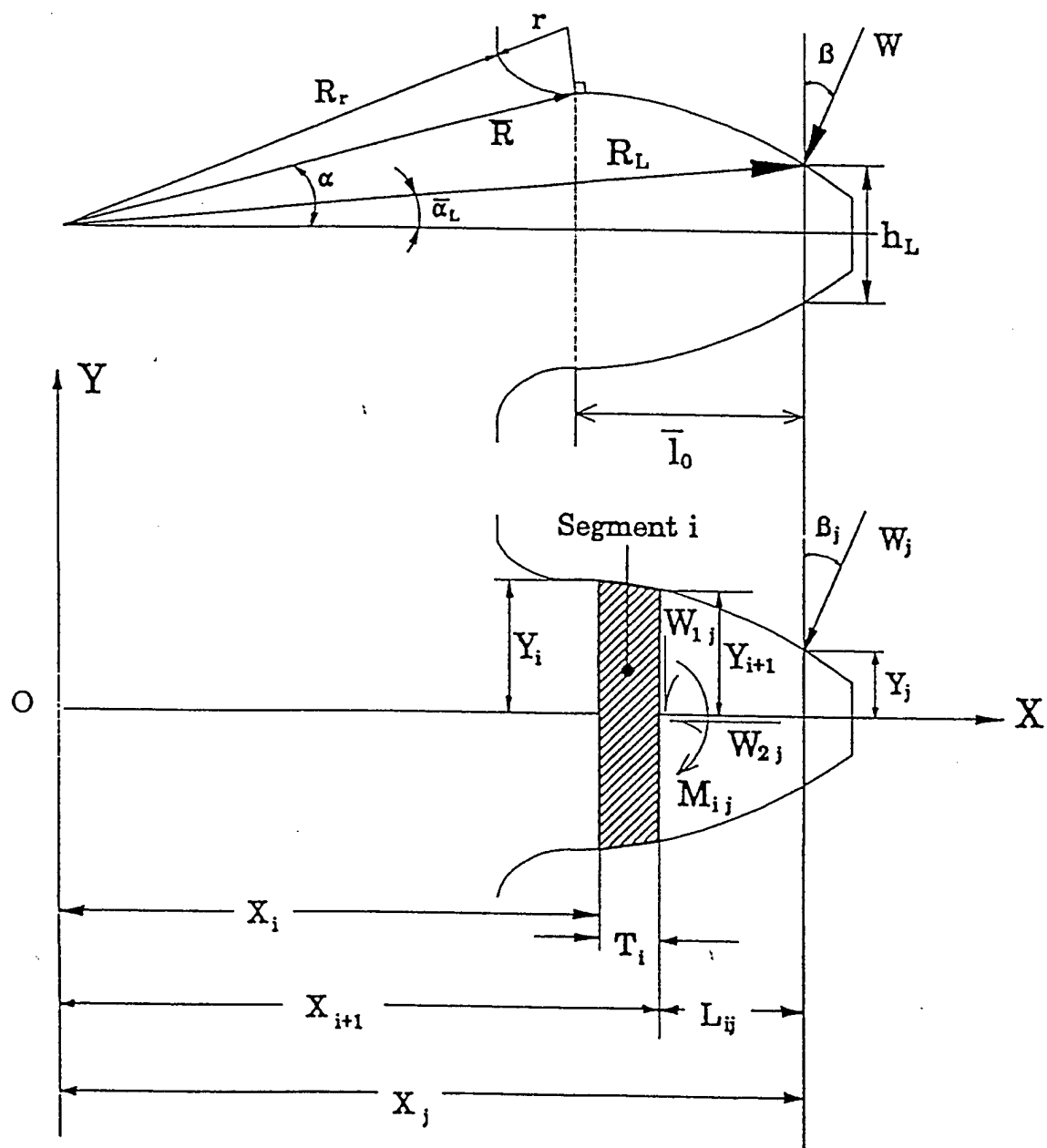detailed illustrations and derivations were presented in the previous works [13] and [14].

12

Figure II.5 Geometry and deflection of an involute portion of a gear tooth

II.3.1 Bending Deflection

(A) Displacement due to $W_j \cos \beta_j$

$$\left(q_W \right)_{ij} = \frac{W_j \cos \beta_j}{3 \, E_e \, I_i} \left(T_i^3 \right) + \frac{W_j \cos \beta_j}{2 \, E_e \, I_i} \left(T_i^2 \, L_{ij} \right) \qquad \textbf{(II.13)}$$

(B) Displacement due to net moments M_{ij}

$$\left(q_M \right)_{ij} = \frac{W_j \left(L_{ij} \cos \beta_j - Y_j \sin \beta_j \right)}{2 \, E_e \, I_i} \left(T_i^2 \right)$$

$$\qquad\qquad\qquad\qquad\qquad\qquad\qquad\qquad \textbf{(II.14)}$$

$$+ \frac{W_j \left(L_{ij} \cos \beta_j - Y \sin \beta_j \right)}{E_e \, I_i} \left(T_i \, L_{ij} \right)$$

where

T_i : thickness of segment i

E_e : "effective Young's module of elasticity"

L_{ij}: the distance from j to i

W_j : the transmitted load

I_i : moment of inertia of segment i

Definition of other variables can be found from Figure II.5.

According to Cornell [5], the value of E_e depends on the tooth width:

For width tooth :

$F / Y > 5$: $E_e = E / (1 - v^2)$

For narrow tooth :

14

$$F / Y < 5 \; : \; E_e = E$$

where Y : the tooth thickness at pitch point

F : tooth face width

n : Poisson's ratio

II.3.2 Shear deformation

The shear deformation is caused by the transverse component of the applied load.

$$\left(q_S \right)_{ij} = \frac{1.2 \; W_j \; T_i \; \cos \beta_j}{G \; A_i} = \frac{2.4 \left(1 + v \right) W_j \; T_i \; \cos \beta_j}{E_e \; A_i} \qquad \text{(II.15)}$$

where

G : shear modulus of elasticity

A_i: cross section area of segment i

II.3.3 Axial Compression

This axial compression due to the component $W_j \sin \beta_j$ is

$$\left(q_C \right)_{ij} = \frac{W_j \; \sin \beta_j \; T_i}{E \; A_i} \qquad \text{(II.16)}$$

The total displacement at the load position j, in the direction of load, due to deformation of segment i can be expressed as:

$$\left(q_1 \right)_{ij} = \left(q_W + q_M + q_S \right)_{ij} \cos \beta_j + \left(q_C \right)_{ij} \sin \beta_j \qquad \text{(II.17)}$$

For a wide tooth plane strain theory is used,

15

$$
(q_1)_{ij} = W_j \left\{ \frac{\cos^2 \beta_j}{E_e} \left[\frac{T_i^3}{3\,I_i} + \frac{T_i^2\,L_{ij} + T_i\,L_{ij}^2}{I_i} \right] \right.
$$

$$
- \frac{\cos \beta_j \, \sin \beta_j}{E_e} \left[\frac{T_i^2\,Y_j}{2\,I_i} + \frac{T_i\,Y_j\,L_{ij}}{I_i} \right]
$$

$$
+ \frac{\cos^2 \beta_j}{E_e} \left[\frac{2.4\,(1 + \nu)\,T_i}{A_i} \right]
$$

$$
\left. + \frac{\sin^2 \beta_j}{E_e} \left[\frac{T_i}{A_i} \right] \right\} \tag{II.18}
$$

For a narrow tooth plane stress theory gives

$$
(q_1)_{ij} = W_j \, \frac{\cos^2 \beta_j \, T_i}{E_e}
$$

$$
\left\{ \frac{\left(\dfrac{T_i^3}{3} + T_i\,L_{ij} + L_{ij}^2 \right) - \tan \beta_j \left(\dfrac{T_i\,Y_j}{2} + T_i\,L_{ij} \right)}{I_i} \right.
$$

$$
\left. + \frac{2.4\,(1 + \nu) + \tan^2 \beta_j}{A_i} \right\} \tag{II.19}
$$

II.3.4 Flexibility of the Fillet and Foundation

The fillet and foundation deflections depend on the fillet geometry as well as the load position and direction. Both the fillet length and angle will affect the deflection. According to the study in Ref. 5, the fillet angle g_f should be taken as 75 degrees and 55 degrees for low contact ratio gears

(LCRG) and high contact ratio gears (HCRG), respectively. As shown in Figure II.6, the

deflections caused by flexibility of fillet and foundation are :

For a plane strain case, wide tooth,

$$
\left(q_{fb} \right)_{ij} = W_j \left\{ \frac{\cos^2 \beta_j}{E_e} \right.
$$

$$
\left[\frac{\dfrac{\left(T_{fb} \right)_i^3}{3} + \left(T_{fb} \right)_i^2 + \left(T_{fb} \right)_i \left(L_{fb} \right)_{ij}}{\left(I_{fb} \right)_i} \frac{2.4 \left(1 + v \right) \left(T_{fb} \right)}{\left(A_{fb} \right)_i} \right]
$$

$$
- \frac{\cos \beta_j \, \sin \beta_j}{E_e} \left[\frac{\dfrac{\left(T_{fb} \right)_i^2 Y_j}{2} + \left(T_{fb} \right)_i Y_j \left(L_{fb} \right)_{ij}}{\left(I_{fb} \right)_i} \right]
$$

$$
\left. + \frac{\sin^2 \beta_j}{E_e} \left[\frac{\left(T_{fb} \right)_i}{\left(A_{fb} \right)_i} \right] \right\}
$$

(II.20)

$$
\left(q_{fe} \right)_{ij} = \frac{W_j \, \cos^2 \beta_j}{E_e \, F} \left(1 - v^2 \right) \left\{ \frac{16.67}{\pi} \left[\frac{\left(l_f \right)_i}{h_f} \right]^2 \right.
$$

$$
+ 2 \left(\frac{1 - v - 2v^2}{1 - v^2} \right) \left[\frac{\left(l_f \right)_i}{h_f} \right]
$$

(II.21)

$$
\left. + 1.534 \left(1 + \frac{\tan^2 \beta_j}{2.4 \left(1 + v \right)} \right) \right\}
$$

For a plane stress case, narrow tooth,

17

$$\left(q_{fb} \right) = W_j \left\{ \frac{\cos^2 \beta_j \left(T_{fb} \right)_i}{E_e} \right.$$

$$\left[\frac{\dfrac{\left(T_{fb} \right)_i^2}{3} + \left(T_{fb} \right)_i \left(L_{fb} \right)_{ij} + \left(L_{fb} \right)_{ij}^2}{\left(I_{fb} \right)_i} \right.$$

$$- \frac{\tan \beta_j \left[\dfrac{\left(T_{fb} \right)_i Y_j}{2} \right] + Y_j \left(L_{fb} \right)_{ij}}{\left(I_{fb} \right)_i}$$

$$\left. \left. + \frac{2.4 \left(1 + v \right) + \tan^2 \beta_j}{\left(A_{fb} \right)_i} \right] \right\}$$

(II.22)

$$\left(q_{fe} \right)_{ij} = \frac{W_j \cos^2 \beta_j}{E_e F} \left(1 + v^2 \right)$$

$$\left\{ \frac{16.67}{\pi} \left[\frac{\left(l_f \right)_i}{h_f} \right]^2 + 2 \left(1 + v \right) \left[\frac{\left(l_f \right)_i}{h_f} \right] \right.$$

(II.23)

$$\left. + 1.534 \left[1 + \frac{\tan^2 \beta_j}{2.4 \left(1 + v \right)} \right] \right\}$$

where

q_{fb} : deflection at and in the direction of load due to beam compliance of fillet.

q_{fe} : deflection due to foundation effects.

Based on the superposition principle, the total deflection at and in the direction of load due to the flexibility of the fillet and foundation can be calculated by adding the above individual deflections, q_{fb} and q_{fe}. That is,

$$\left(q_F \right)_{ij} = \left(q_{fb} \right)_{ij} + \left(q_{fe} \right)_{ij}$$

(II.24)

18
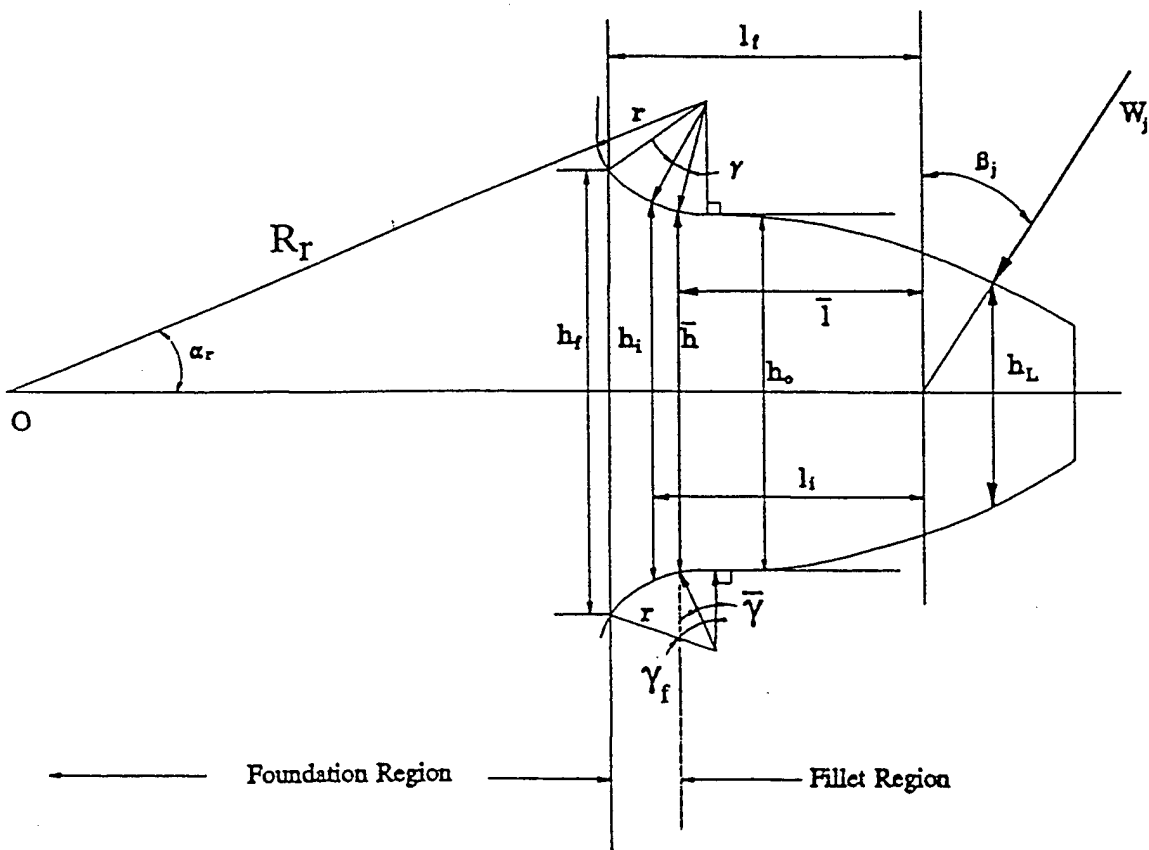
Figure II.6 Flexibility of fillet and foundation

II.3.5 Local Contact Deflection

The local deflection is caused by line-contact and compression deformations. According to Palmgren's study [15], a semi-empirical formula (equation II.25) was developed for contact compliance of cylinders in rolling bearings. The local contact deflection of meshing teeth can be computed using the formula without significant error. Since the contact conditions for a pair of meshing gears are similar to that for a rolling bearing.

$$(q_L)_{ij} = \frac{1.275}{E_{12}^{0.9} \; F^{0.8} \; W_j^{0.1}} \qquad \text{(II.25)}$$

$$E_{12} = \frac{2 \; E_1 \; E_2}{E_1 + E_2} \qquad \text{(II.26)}$$

where E_1, E_2 are Young's modulus of elasticity of gears.

II.3.6 Tooth Stiffness

If meshing portion of the tooth is divided into n segments, then, for each segment, the total deflection $(q_T)_j$ can be computed as:

$$(q_T)_j = \sum_{i=1}^{n} \left[(q_W)_{ij} + (q_M)_{ij} + (q_L)_{ij} \right] \qquad \text{(II.27)}$$

Furthermore, by multiplying the reciprocal of $(q_T)_j$ with the shared tooth load W_j at j position, the equivalent tooth meshing stiffness for each segment can be expressed as the ratio of transmitted load to the total deflection. Since there are n segments involved, the total stiffness can be summed to determine the average tooth meshing stiffness $(K_G)_{avg}$ from the following equations:

20

$$(K_G)_J = \frac{W_j}{(q_T)_j} \qquad\qquad \text{(II.28)}$$

$$(K_G)_{avg} = \frac{1}{n} \sum_{i=1}^{n} (K_G)_i \qquad\qquad \text{(II.29)}$$

where n is the meshing position number.

Because the mass of a rotating gear body is theoretically concentrated at the radius of gyration, the deflection reference used in this study is assumed to be at this radius. The theoretical deflection and stiffness of the gear teeth will be affected by changing the mass moment of inertia and the geometry of the gear body.

II.4 Gear Tooth in Action

Figure II.7 shows a pair of gears with a contact ratio 1.40. A driving pinion tooth is just coming into contact at point E on the right and the preceding tooth on the left is in contact at point G. It should be noted that the contact starts at E and ends at H, where the outside diameter of the gear or the pinion intersect the line of action. When the gears rotate, the contact point of the tooth pair T_{G2} moves from point E to point F. Likewise, tooth pair T_{G1} moves from point G to point H, respectively. Thus, two pairs of teeth carry the load during this period. When the contact point of tooth pair T_{G1} passes point H, this tooth pair loses contact, leaving only one pair of teeth T_{G2} to carry the load. As the gears continue turning, the tooth pair T_{G3} starts contact at point E. Again, two pairs of teeth T_{G2} and T_{G3} carry the load until tooth pair T_{G2} leaves contact at point H. The position of the contact point of gear teeth along the line of action usually is expressed in term of roll angles of the driving gear. This expression is also consistent with our

21
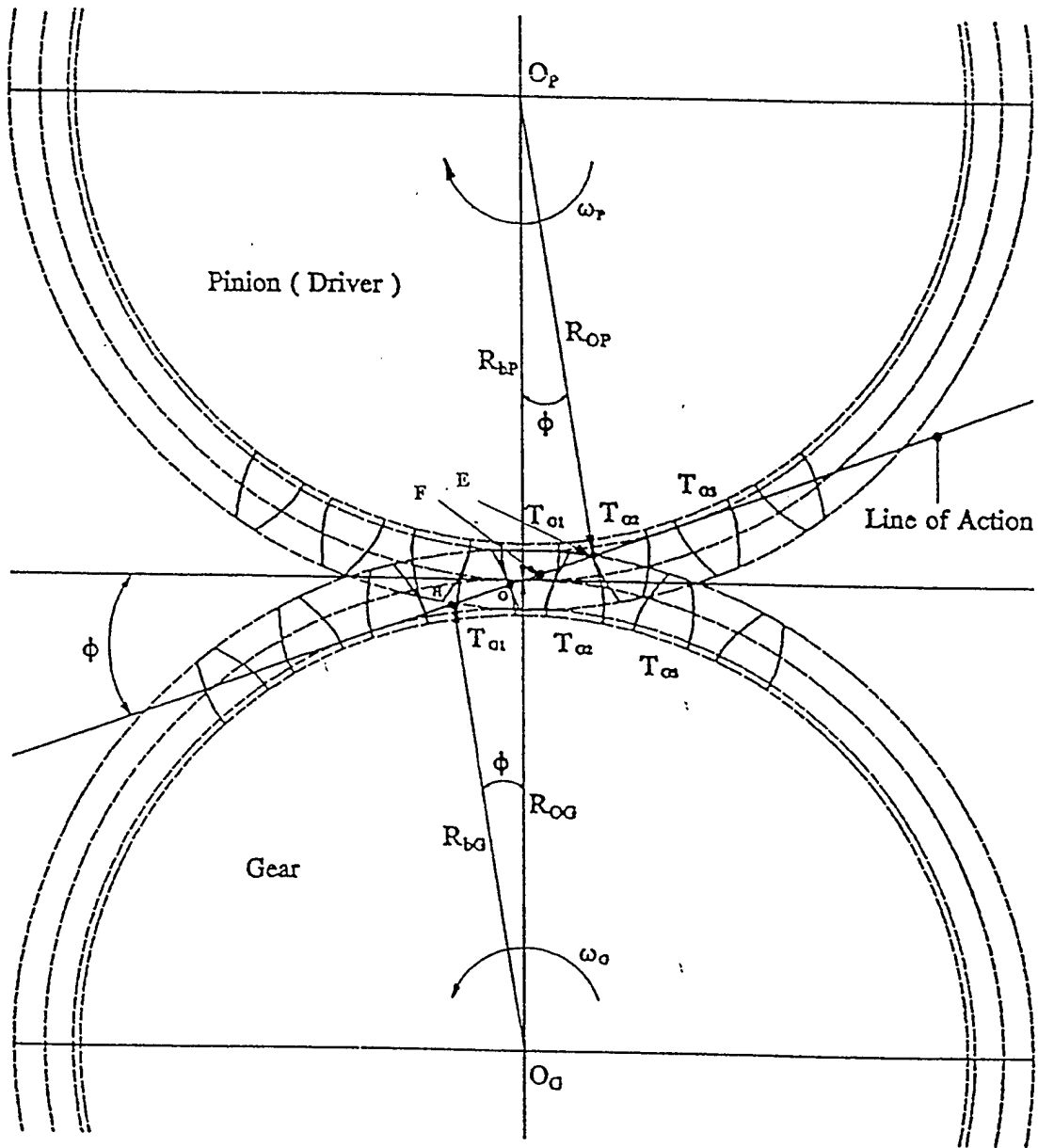
Figure II.7 Illustration of gear teeth meshing action

gear tooth deflection and stiffness calculations, since they are also expressed in roll angles of the driving gear.

II.5 Transmission Error and Load Sharing

The transmission error (TE) is defined as the departure of a meshed gear pair from a constant angular motion. TE may be defined as the instant deviation of the following gear from an ideal nominal value. TE is a result of many contributors and the main items are:

(A) Combined deflection of meshing teeth

(B) Tooth spacing error

(C) Tooth profile error

(D) Runout error

The total transmission error for a gear pair is the sum of individual errors caused by above-mentioned sources and is written as:

$$
\left(E_T^k \right)_j = \left(\sum_{r=1}^{2} {}_d E_r^k \right)_j + \left(\sum_{r=1}^{2} {}_p E_r^k \right)_j + [\, P \,] \left(\sum_{r=1}^{2} {}_s E_r^k \right)_j
$$

$$(II.30)$$

where

k : the mating tooth pairs in sequence

r : driving and driven gears

P : if $k = 1$ then $P = 0$, otherwise $P = 1$

${}_d E$: deflection of gear teeth at contact point

${}_p E$: tooth profile error

${}_s E$: tooth spacing error

23

Since the transmission error is the same for each tooth pair sharing the total transmitting load (W), it can be expressed as:

$$\left(E_T^1 \right)_j = \left(E_T^2 \right)_j = \ldots \tag{II.31}$$

$$W = \sum_{n=1}^{(CR)+1} W_j^n \tag{II.32}$$

where (CR) is the integer part of the contact ratio.

The magnitude of the load shared by each individual tooth pair can be calculated by solving a set of simultaneous equations (II.30, II.31, and II.32). It should be noted that the meshing analysis equations are only valid under the assumption that there are n tooth pairs simultaneously in contact during mesh. If any of the tooth pairs lose contact, the terms corresponding to the tooth pairs that lose contact are eliminated. Then, the remaining equations are solved for the load and static transmission error of the tooth pairs that are still in contact.

II.6 Torque Due to Friction in the Mesh Gears

There is no general agreement for the friction coefficient. Some semi-empirical formulas have been developed based on different assumptions. Two of these formulas, Buckingham's [25], and Anderson and Loewenthal's formulas [26], were used in this study to determine the friction torques which will be incorporated into the equations of motion for dynamic analysis in a later chapter.

Buckingham's formula:

$$f = \frac{0.05}{e^{0.125 \, V_s}} + 0.002 \sqrt{V_s} \tag{II.33}$$

$$f_a = \frac{4 \, f}{3} \tag{II.34}$$

$$f_r = \frac{2f}{3} \qquad\qquad (II.35)$$

where

  f : average coefficient of friction

  f_a : average coefficient of friction of approach

  f_r : average coefficient of friction of recess

  V_s : sliding velocity, ft/min

Anderson and Loewenthal's formula:

$$f = 0.0127 \log \frac{45.4\,W}{F\ U_0\ V_s\ V_R^2} \qquad\qquad (II.36)$$

$$V_R = 0.2094\,n\ R_{P1}\left[\sin\phi - \left(S\ \frac{(m_g - 1)}{2\ R_{P1}} \right) \right] \qquad\qquad (II.37)$$

where

  f : average coefficient of friction

  W : actual applied load, lb

  F : tooth face width, in

  V_s : sliding velocity, in/sec

  V_R : rolling velocity, or sum velocity, in/sec

  u_0 : lubricant absolute viscosity, lbf-sec/in^2

  S : absolute distance, in, from pitch point to contact point along the line of action

  n : rotating speed, rpm

  m_g : gear ratio

Based on these two formulas, the friction coefficient can be estimated. By taking into account the shared tooth load, the frictional torque T_f on each individual gear shaft can be found. This torque varies along the path of contact and changes direction at the pitch point.

II.7 Flexible Shaft and Rolling Element Bearing

Shafts and bearings are major components of the gear system. The most elementary rolling element bearing-shaft assembly is shown in Figure II.8. Figure II.9 shows a similar assembly with a overhung load. The concentrated load P is transmitted between gears along the contact-line direction. Figure II.10 shows the free body diagrams of the force acting on two mating gears. The system is statically determinate, thus, the force F_{PG} exerted on the driven gear causes a reaction force P as well as a torque T. The force P produces a shaft deflection and the torque T keeps the gear rotating. To obtain shaft deflection, a shaft can be considered as either a simply supported beam or a cantilever beam model, it depends on gear mounting position. From mechanics-of-materials, the shaft deflection can be calculated as:

$$q_G = \frac{P\,a\,b}{6\,E\,I\,l}\left(a^2 + b^2 + l^2\right) \qquad\qquad (\text{II.38})$$

for a gear mounted between two bearings.

$$q_G = -\frac{P\,a^2}{3\,E\,I}\left(1 + a\right) \qquad\qquad (\text{II.39})$$

for a gear mounted outside two bearings.
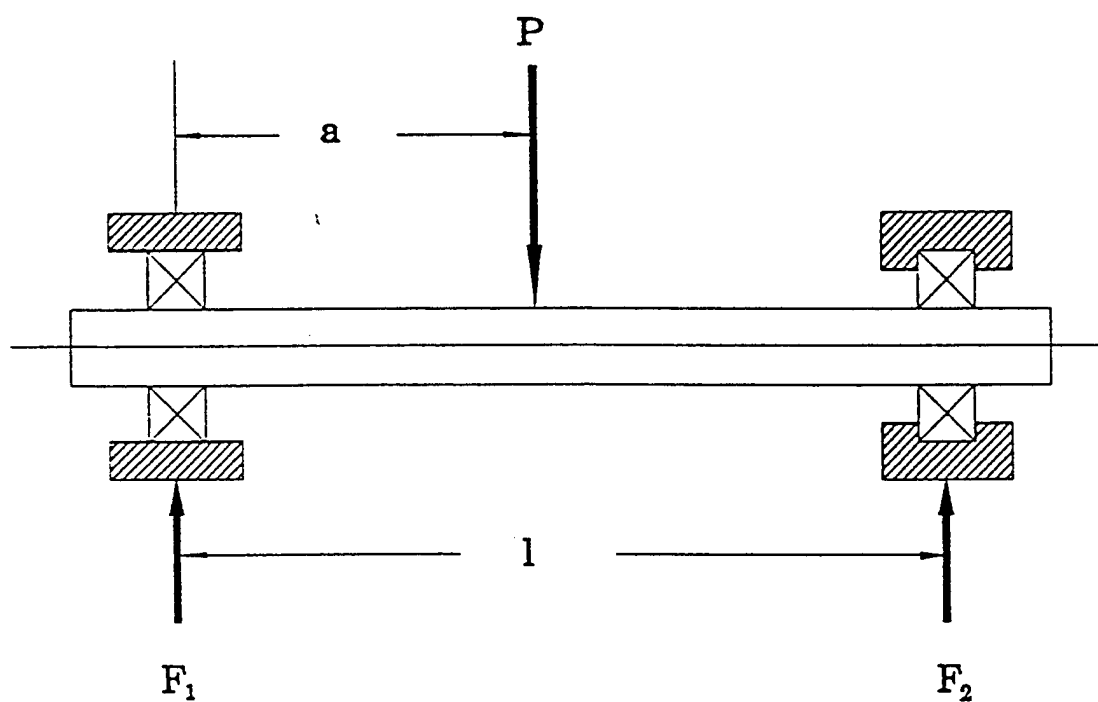
Figure II.8 A simple two-bearing-shaft system
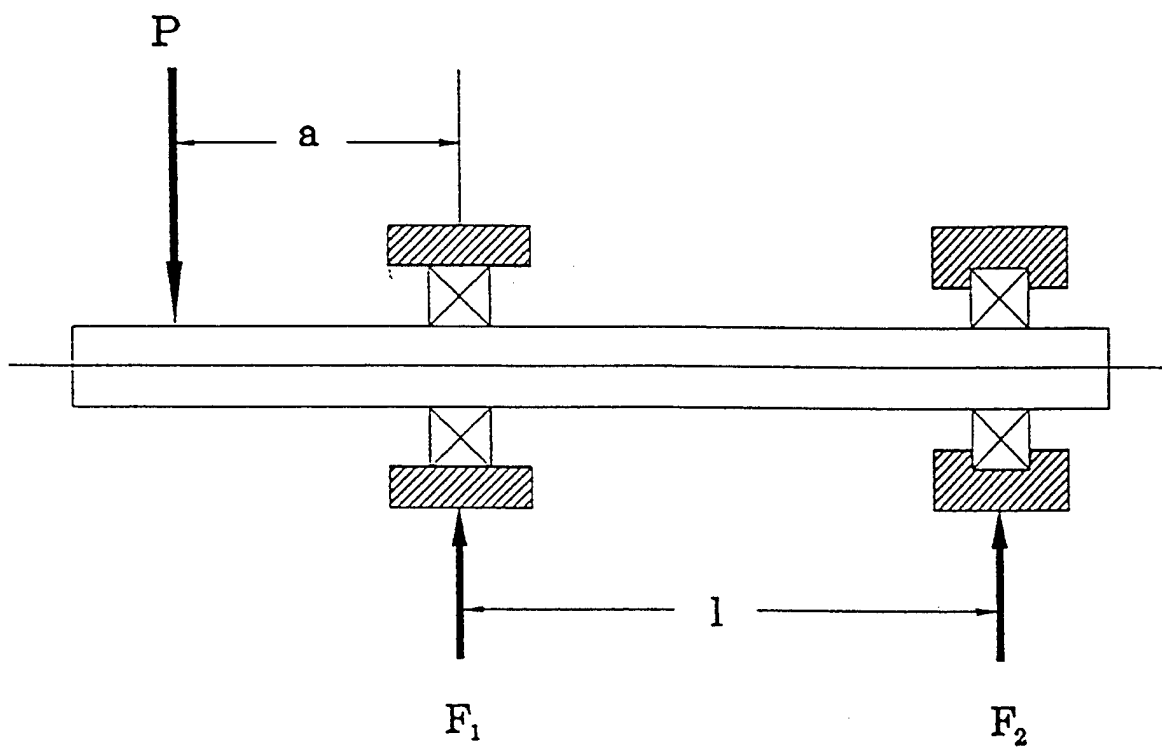
Figure II.9 A simple two-bearing-shaft system, overhung load
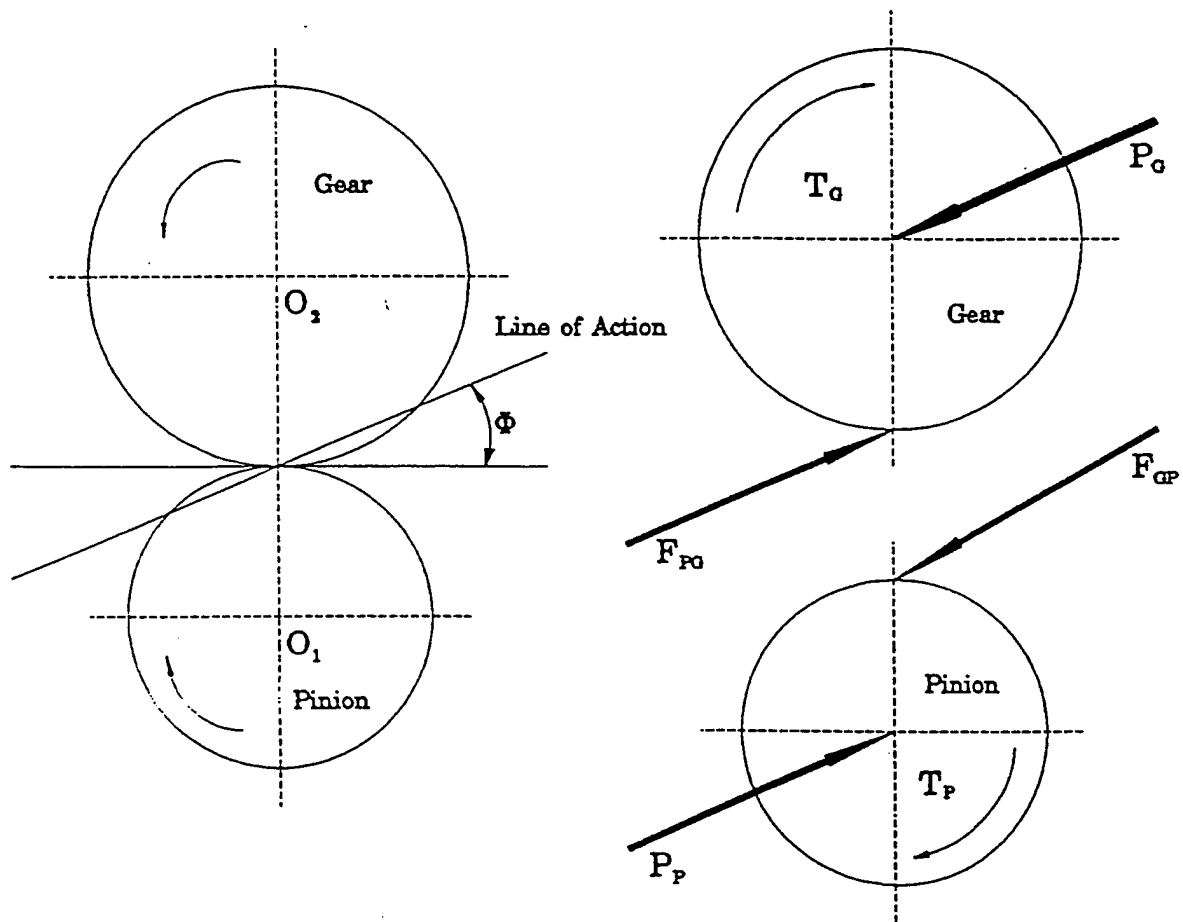
Figure II.10 Free-body diagrams of the forces acting upon two gears
in a simple gear train

Usually, when a rotor system is analyzed for deflections, bearings are assumed to be rigid. In fact the bearings deflect when subjected to a load, which adds to the shaft deflection. For a rolling bearing in service, the rolling element presses against its race-way either at a point or along a line, depending on the type of bearing. Under an external force, the rolling element deforms and the associated contact area is dependent upon the load magnitude as well as the curvature of the rolling element. On the basis of Hertz's "Contact of Elastic Solids" theory, Garguilo [16] derived a series of formulas to calculate deflection for different types of bearings. These formulas are expressed as follows:

For a deep-groove or angular-contact radial ball bearing:

$$\delta_r = 46.2 \times 10^{-6} \sqrt[3]{\frac{F_r^2}{D \ Z^2 \ \cos^5 \alpha}} \qquad \text{(II.40)}$$

For a Self-aligning ball bearing:

$$\delta_r = 74.0 \times 10^{-6} \sqrt[3]{\frac{F_r^2}{D \ Z^2 \ \cos^5 \alpha}} \qquad \text{(II.41)}$$

For a spherical roller bearing:

$$\delta_r = 14.5 \times 10^{-6} \sqrt[3]{\frac{F_r^3}{L^2 \ Z^3 \ \cos^7 \alpha}} \qquad \text{(II.42)}$$

For a straight roller or tapered roller bearing:

$$\delta_r = 3.71 \times 10^{-6} \frac{F_r^{0.9}}{L^{0.8} \ Z^{0.9} \ \cos^{1.9} \alpha} \qquad \text{(II.43)}$$

30

where

       d_r : bearing deflection, in

       D : rolling element diameter, in

       Z : number of rolling elements

       a : Contact angle, rad

       L : roller effect length

       F_r : radial external force, lb

When a gear pair is in operation, shaft and bearing deflections cause the center of gear rotation to shift along the direction of the line of action (Figure II.11) from its original location. The shift increases the center distance and pressure angle of the meshing gears, which in turn reduces the contact ratio. Since shaft and bearing deflections are usually small, their influence is often neglected.

To evaluate system dynamics, the shaft and connected masses should be taken into consideration. These parameters, polar mass moment of inertia, stiffness of shaft, and stiffness of connected masses, are incorporated into the equations of motion in the dynamic analysis. As suggested in [17], the polar mass moment of inertia J and the torsional stiffness K can be calculated by:

$$J = \frac{\pi \, l \, \rho}{32} \left(D_o^4 - D_i^4 \right) \qquad\qquad \textbf{(II.44)}$$

$$K = I \times G = \frac{\pi \, G}{32} \left(D_o^4 - D_i^4 \right) \qquad\qquad \textbf{(II.45)}$$

where

r : mass density, lb/in^3

D_o : outside diameter of shaft, in

D_i : inside diameter of shaft, in

l : length of shaft, in

I : torsional constant, in^4

G : shear modules, lb/in^2
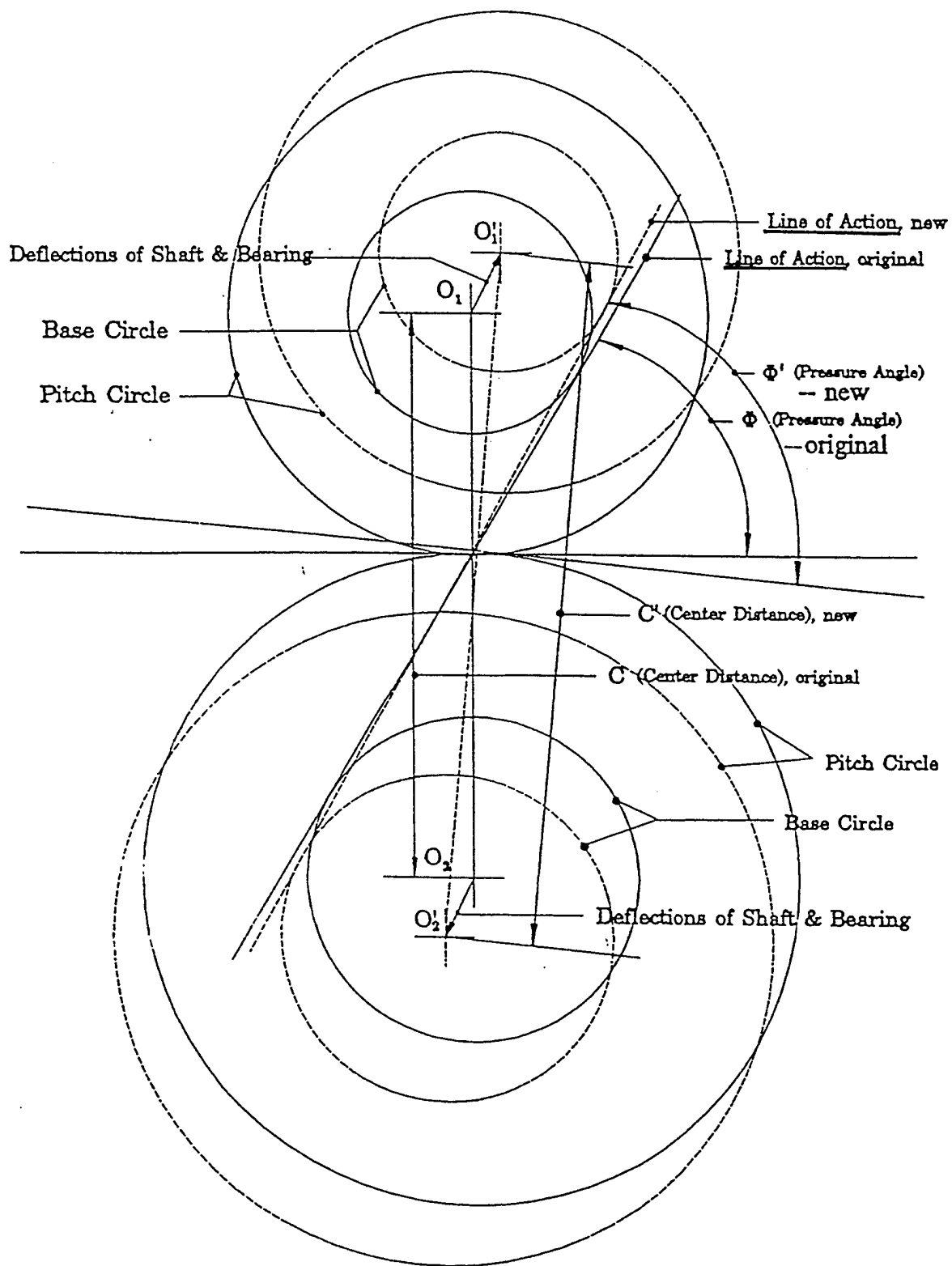
Figure II.11 Shifting of center of gear rotation with deflections of shaft and bearing

CHAPTER III

SYSTEM DYNAMIC ANALYSIS

III.1 Equations of Motion

To precisely model the dynamic loading is a difficult task, even in idealized geometry conditions. The vibration of a gear tooth is affected by the tooth force which fluctuates in amplitude, direction, and position during the meshing process. Load fluctuations are influenced by the damping effect of the lubricant and the operating speed. In general, a gear train is very complicated and composed of various sub-systems, such as motor, bearing, shaft, ..., etc. and each sub-system is a complete dynamic system. The gear transmission is generally simplified to a relatively small number of lumped masses connected elastically. Under this modeling, a simple spur gear system shown in Figure III.1 can be represented by a mathematical model shown in Figure III.2. This model has four degrees of freedom and consists of gears, input device, output device, and two flexible shafts. The dynamic behavior of meshing gears could be considered as a periodic forced motion. To develop the governing equations, some assumptions are applied in addition to those made at the beginning of chapter II. These assumptions are:

(A) Damping (due to material in gears and shafting and from lubrication) is expressed as a constant damping coefficient.

(B) The differential equations of motion are expressed along the theoretical line of action.

(C) The reference point for tooth deflection is assumed to be located along the tooth centerline at the radius of gyration of the gear body.
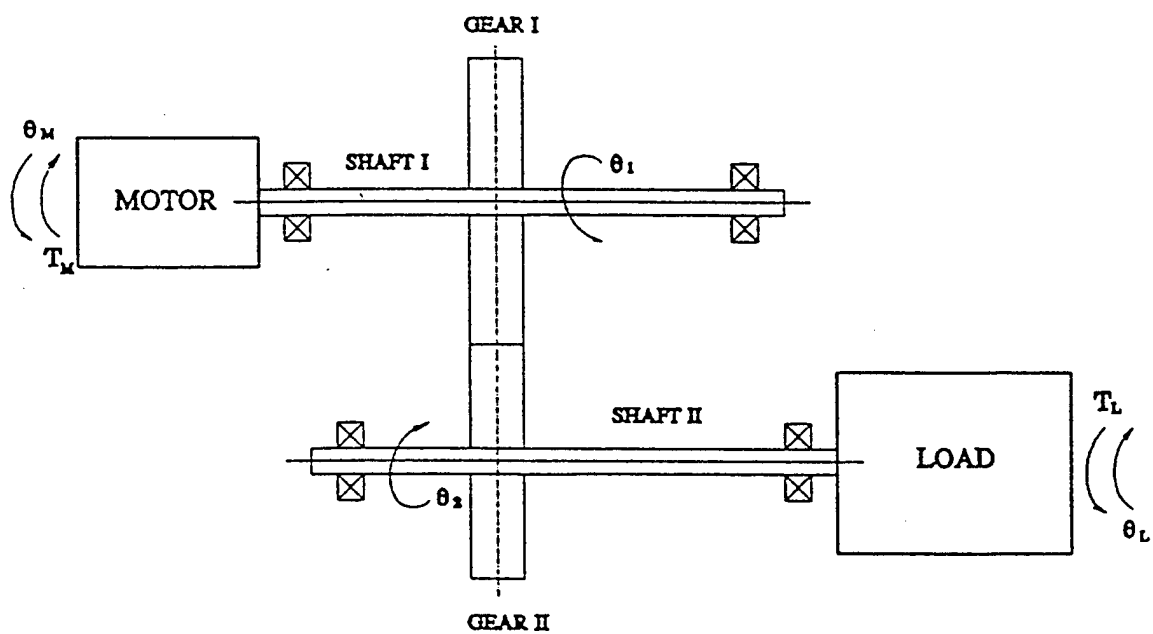
Figure III.1   A simple spur gear train with two parallel shafts
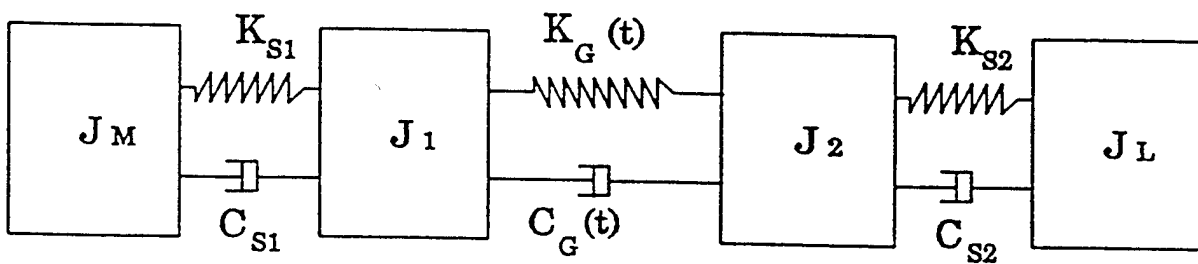
Figure III.2 Mathematical model of a simple spur gear system

Using basic gear geometry and elementary vibration principles, the governing equations can be expressed as follows:

$$J_M \ddot{\theta}_M + C_{s1}(\dot{\theta}_M - \dot{\theta}_1) + K_{s1}(\theta_M - \theta_1) = T_M \qquad \text{(III.1)}$$

$$J_1 \ddot{\theta}_1 + C_{S1}(\dot{\theta}_1 - \dot{\theta}_M) + C_G(t)\left[R_{b1}(R_{b1}\dot{\theta}_1 - R_{b2}\dot{\theta}_2) \right]$$

$$+ K_{S1}(\theta_1 - \theta_M) + K_G(t)\left[R_{b1}(R_{b1}\theta_1 - R_{b2}\theta_2) \right] = T_{F1}(t)$$

$$\text{(III.2)}$$

$$J_2 \ddot{\theta}_2 + C_{S2}(\dot{\theta}_2 - \dot{\theta}_1) + C_G(t)\left[R_{b2}(R_{b2}\dot{\theta}_2 - R_{b1}\dot{\theta}_1) \right]$$

$$+ K_{S2}(\theta_2 - \theta_1) + K_G(t)\left[R_{b2}(R_{b2}\theta_2 - R_{b1}\theta_1) \right] = T_{F2}(t)$$

$$\text{(III.3)}$$

$$J_L \ddot{\theta}_L + C_{S2}(\dot{\theta}_L - \dot{\theta}_2) + K_{S2}(\theta_L - \theta_2) = -T_L \qquad \text{(III.4)}$$

where

J_M, J_1, J_2, J_L : mass moments of inertia for motor, gear I, gear II, and load, respectively

$K_{S1}, K_{S2}, K_G(t)$: stiffnesses of shaft I, shaft II, and gear teeth, respectively

$C_{S1}, C_{S2}, C_G(t)$: damping coefficients of shaft I, shaft II, and gears

$T_{F1}(t), T_{F2}(t)$: friction torque of driving gear and driven gear

T_M, T_L : input and output torque

The time varying friction torque of the gears and periodic variation of the mesh stiffness act as excitation terms to the equation of motion. The stiffness of gear teeth (represented by springs)

is determined by the method developed in Chapter II. The system dynamic characteristics can then be found by solving the above simultaneous differential equations.

III.2 Numerical Solution Approach

Due to nonlinearity in the equation of motion, it is necessary to apply a numerical approach to find the solution. Two steps are used in solving the equations. First, a static analysis is introduced to obtain the required parameters. Second, a dynamic analysis is incorporated to obtain the final result.

The static analysis includes the following: the geometry of meshing gears is determined from basic gear dimensions, the center distance of meshing gears affected by shaft and bearing deflections is calculated by using equations mentioned in Chapter II, the transmission error, load sharing, and tooth stiffness obtained by those procedures referred in Chapter II.

The dynamic analysis is conducted as follows. The fluctuating output torque, damping in gears, frictional torque, and time-varying mesh stiffness under constant input torque are taken into consideration. Initial values of angular displacement and angular velocity are needed in the analysis. Starting values are obtained through preloading the input shaft with the output shaft fixed. The preload torque is the static design torque carried by the system.

The equations of motion are linearized by dividing the mesh period into many equal intervals. Those equations are solved by an iteration technique incorporating the nominal initial values. At each step X_n and V_n need to be compared respectively with the initial value X_0 and V_0 to confirm the iteration convergence. To determine whether the convergence is satisfied, the following criterions are used:

$$| X_n - X_0 | \leq 0.05 X_0 \quad ,$$

and

$$| V_n - V_0 | \leq 0.05 \, V_0 \quad ,$$

The same steps are repeated by averaging the initial and calculated values of angular displacement X_n, and angular velocity V_n, as the new initial values of next period, respectively.

Three situations may occur when gears are in mesh. Each one of these three situations (A, B, or C) will produce a specific dynamic condition. Assume gear 1 is the driving gear,

Case (A) $R_{b1} \, \theta_1 - R_{b2} \, \theta_2 > 0$

This is normal operation case. The dynamic tooth load on gear 1 is then:

$$W_{d1} = K_G(t)\left(R_{b1} \, \theta_1 - R_{b2} \, \theta_2 \right) + C_G(t)\left(R_{b1} \, \dot{\theta}_1 - R_{b2} \, \dot{\theta}_2 \right)$$

(III.5)

which is the same as the dynamic tooth load on gear 2,

$$W_{d2} = W_{d1}$$

(III.6)

Case (B) $R_{b1} \, \theta_1 - R_{b2} \, \theta_2 \leq 0$ and $\left| R_{b1}\theta_1 - R_{b2}\theta_2 \right| \leq B_h$

In this case, the gears will separate and lose contact, therefore,

$$W_d = 0$$

(III.7)

Case (C) $R_{b1} \; \theta_1 \; - \; R_{b2} \; \theta_2 \; \leq \; 0$ and $\left| R_{b1}\theta_1 - R_{b2}\theta_2 \right| > B_h$

In this case, gear 2 will collide with gear 1 on the backside. The dynamic tooth load on gear 1 is

$$W_{d1} \; = \; K_G \; (t) \left[\left(R_{b1} \; \theta_1 \; - \; R_{b2} \; \theta_2 \; \right) - B_h \right] \; + \; C_G \; (t) \left(R_{b1} \; \dot{\theta}_1 \; - \; R_{b2} \; \dot{\theta}_2 \; \right)$$

(III.8)

and

$$W_{d2} \; = \; W_{d1}$$
(III.9)

The term $(\; R_{b1} \; \theta_1 \; - \; R_{b2} \; \theta_2 \;)$ is the relative dynamic displacement between gear 1 and gear 2, and B_h is the backlash of gears.

In general, damping is present in an oscillatory system. The mathematical description of damping effect is so complicated that it needs to be simplified in the vibration analysis. A simplified damping model is introduced in this study to determine the effective damping factor C_{s1} and C_{s2},

$$C_{S1} \; = \; 2 \; \xi_{S1} \sqrt{\dfrac{K_{S1}}{\left(\dfrac{1}{J_D} + \dfrac{1}{J_1} \right)}}$$

(III.10)

$$C_{S2} \; = \; 2 \; \xi_{S2} \sqrt{\dfrac{K_{S2}}{\left(\dfrac{1}{J_L} + \dfrac{1}{J_2} \right)}}$$

(III.11)

The ξ represents the damping ratio of shafts (expressed as a fraction of critical damping). Based on experimental results [18], the damping in the shafts due to material damping was found to be between 0.005 and 0.007. In this study, it is taken as 0.005.

For damping between the gear teeth, similar formulas are used:

$$C_{G1} = 2\xi \sqrt{\frac{K_{G1}}{\left(\dfrac{R_{b1}^2}{J_1} + \dfrac{R_{b2}^2}{J_2}\right)}} \qquad \text{(III.12)}$$

$$C_{G2} = 2\xi \sqrt{\frac{K_{G2}}{\left(\dfrac{R_{b1}^2}{J_1} + \dfrac{R_{b2}^2}{J_2}\right)}} \qquad \text{(III.13)}$$

[19] and [20] indicated that the value of the damping ratio ξ for these formulas is between 0.03 to 0.17. An average value of 0.10 is used in our study. The flow chart for the above numerical approach is shown in Figure III.3.

III.2.1 Undamped Natural Frequency

The undamped equations of motion for the gear pair in mesh can be obtained by neglecting the damping and excitation terms from Equations III.1 through III.4. The undamped equations of motion were solved by a Jacobian iteration technique to find the natural frequencies of the system.

In equation III.14 the average gear mesh stiffness $(K_G)_{avg}$ is introduced to facilitate the solution for eigenvalues. $(K_G)_{avg}$ is determined by summing up the discrete stiffness values over one tooth mesh cycle and dividing by the number of mesh positions in the cycle.

Geometry of system components, conditions of system operation.

↓

Shaft and bearing deflections, re-calculate relative conditions of system operation.

↓

Calculation of static and initial conditions.

↓

Calculation of dynamic condition for one period per mesh.

↓

$| X_n - X_o | \leq 0.05\ X_o$

and

$| V_n - V_o | \leq 0.05\ V_o$

No →

$X_o = (X_n + X_o) / 2$

$V_o = (V_n + V_o) / 2$

Yes ↓

Calculation of dynamic load and stress.

↓

Output of result
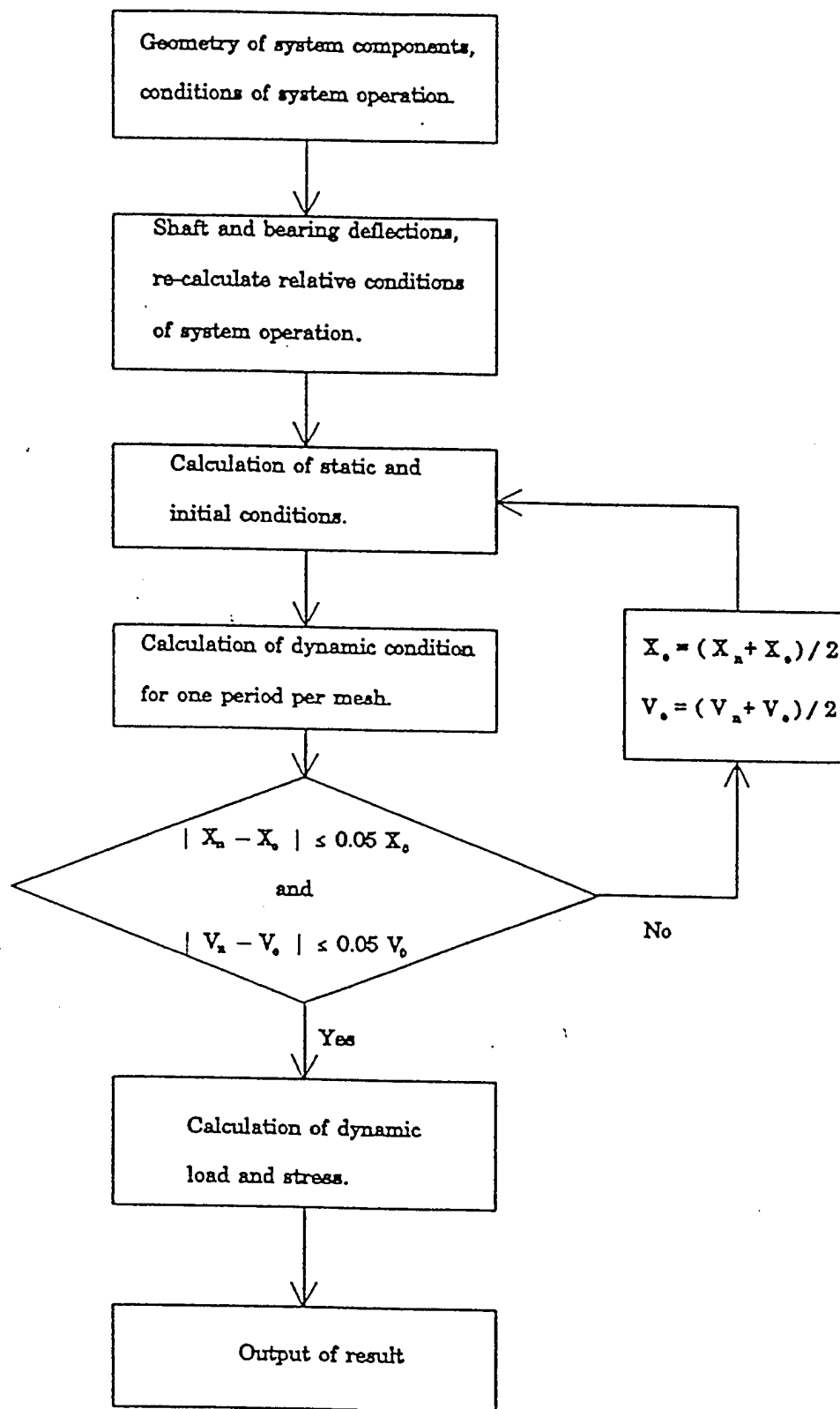
Figure III.3 Flow chart for computation procedure

$$\begin{bmatrix} J_M & 0 & 0 & 0 \\ 0 & J_1 & 0 & 0 \\ 0 & 0 & J_2 & 0 \\ 0 & 0 & 0 & J_L \end{bmatrix} \begin{bmatrix} \ddot{\theta}_M \\ \ddot{\theta}_1 \\ \ddot{\theta}_2 \\ \ddot{\theta}_L \end{bmatrix} + \begin{bmatrix} k_{S1} & -k_{S1} & 0 & 0 \\ -k_{S1} & k_{S1} + (k_G)_{avg} R_{b1}^2 & -(k_G)_{avg} R_{b1} R_{b2} & 0 \\ 0 & -(k_G)_{avg} R_{b1} R_{b2} & k_{S2} + (k_G)_{avg} R_{b2}^2 & -k_{S2} \\ 0 & 0 & -k_{S2} & k_{S2} \end{bmatrix} \begin{bmatrix} \dot{\theta}_M \\ \dot{\theta}_1 \\ \dot{\theta}_2 \\ \dot{\theta}_L \end{bmatrix} = [0]$$

(III.14)

III.2.2 Fast Fourier Transform of Transmission Error

According to Mark [21], gear noise and gear dynamic load are often characterized by strong components at the tooth mesh frequency. Kubo [22] stated that the magnitude of gear transmission error at the harmonics of the tooth mesh frequency corresponds somewhat proportionately to the magnitude of maximum dynamic tooth fillet stress. Both of these phenomena are caused by vibrational excitations due to time-varying stiffnesses of meshing gears. Therefore, the dynamic response also corresponds proportionately to tooth mesh frequency. In this study, frequency analysis of static transmission error is performed by taking the fast Fourier transform (FFT) of its time wave. In general, the amplitudes of higher harmonics are usually small, thus their contribution to the excitation be neglected. Therefore, only the first twelve harmonic values are calculated. A typical plot of the static transmission error spectrum is shown in Figure III.4.

III.2.3 Speed Survey of Dynamic Stress and Load Factor

Cornell [23] modified a formula developed by Heywood [24] for the calculation of root fillet bending stress of a gear tooth. This formula is readily adapted to the geometry of involute gear teeth and can be expressed as

43

FFT – TRANSMISSION ERROR
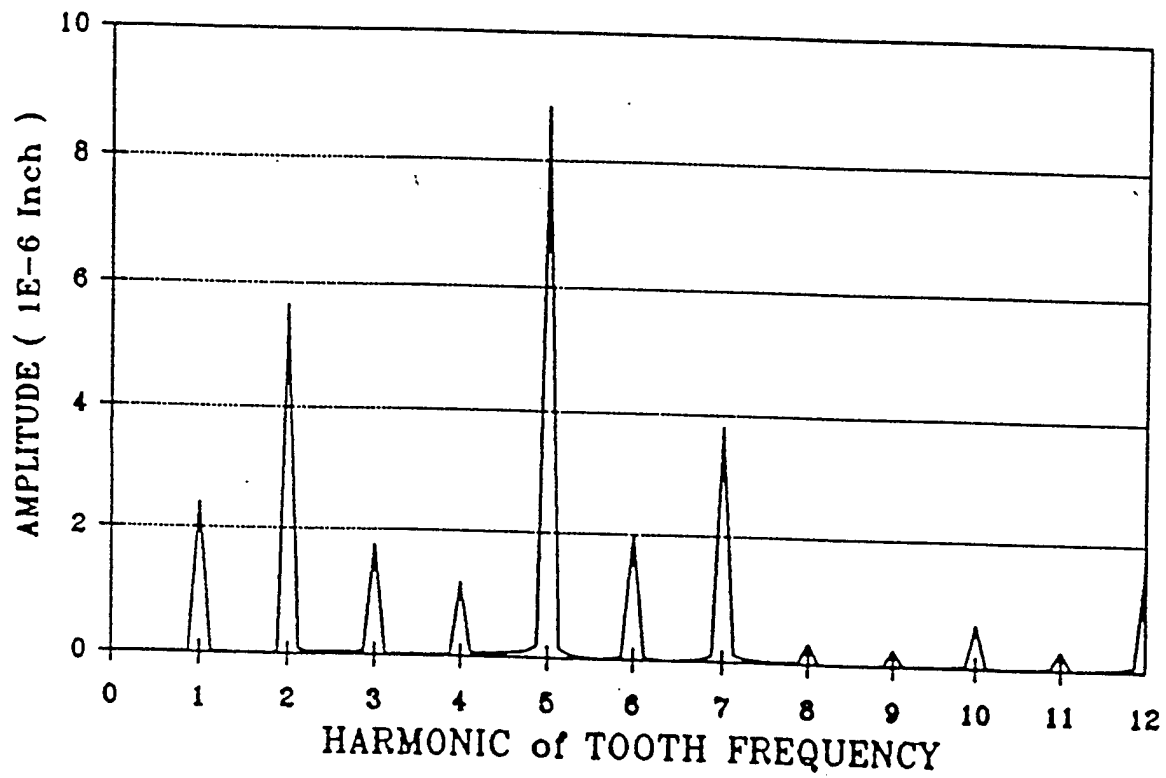
Figure III.4 Frequency spectrum of static transmission error

$$\sigma_j = \frac{W_j \, \cos \, \beta_j}{F} \left[1 + 0.26 \left(\frac{h_s}{2 \, r} \right)^{0.7} \right]$$

$$\left\{ \frac{6 \, l_s - \left(\dfrac{h_L \, \tan \, \beta_j}{2} \right)}{h_s^2} + \left(\frac{0.72}{h_s \, l_s} \right)^{0.5} \right. \qquad\qquad \textbf{(III.15)}$$

$$\left. \left(1 - \frac{h_L}{h_s} \, v \, \tan \, \beta_j \right) \frac{\tan \, \beta_j}{h_s} \right\}$$

where

v : approximately 1/4 according to Heywood [24]

β_j : the load angle, degree

F : face width of gear tooth, in

r : fillet radius, in

and the rest of nomenclature is defined in Figure III.5. Note that γ_s, which defines the position of

maximum fillet stress, is 30 degrees for LCRG, and 20 degrees for HCRG, as suggested by

Conell [23].

The main source of gear vibration is the time-varying tooth stiffness due to alternating

tooth load, and changing tooth contact position. To investigate the dynamic performance of a

gear system under realistic operating conditions, the rotating speeds were varied over a wide

range. Figure III.6 shows the variation of gear load and tooth root stress as a function of

operating speed for a typical high-contact-ratio gear pair. The load and stress are shown in

nondimensional form as the dynamic load factor, which is the ratio of maximum dynamic load to

total applied load, and the dynamic stress factor, which is the ratio of maximum dynamic stress
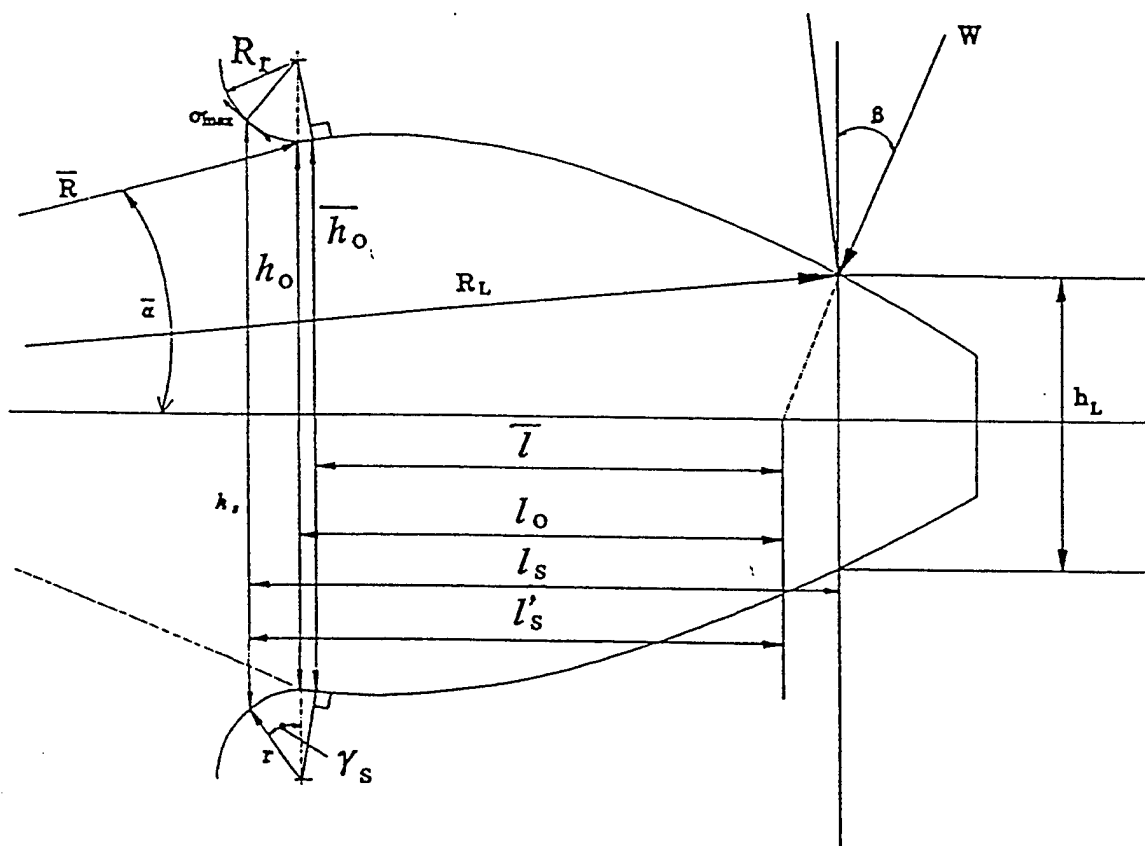
Figure III.5 Nomenclature for modified Heywood formula
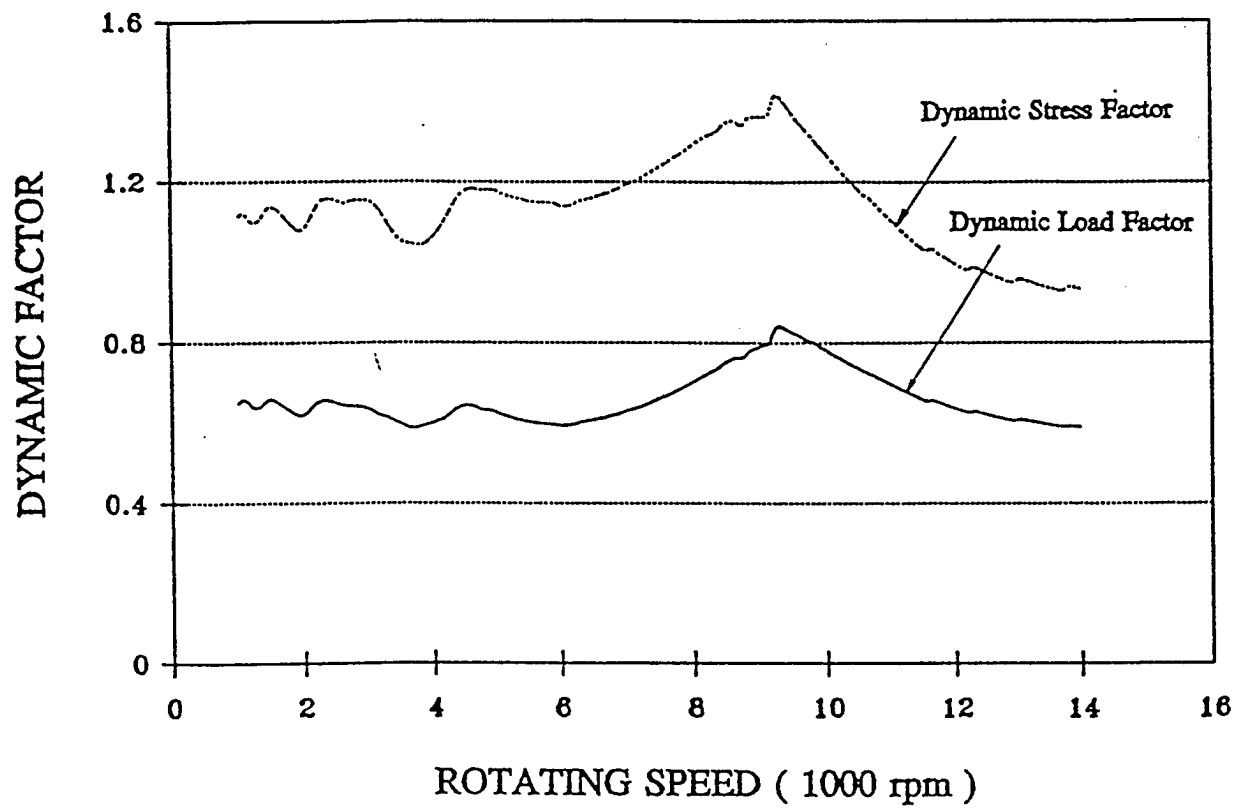
Figure III.6   Speed survey of dynamic load factor and dynamic stress factor

to maximum static stress. The total applied load is the input torque divided by the base radius of the driving gear. It is found that the major peak for both dynamic stress and dynamic load factors occurs near 9300 rpm, which is the system natural frequency.

The analysis described above has been incorporated into the NASA gear dynamics program DANST. The program calculates the properties of system components and substitutes them into bending stresses and other parameters. DANST was used for the parameter study which follows.

CHAPTER IV

PARAMETER STUDY

IV.1 Effect of Damping

The Damping ratio ξ_g governing the dynamic load variation depends on the viscous friction and the material properties of the meshing gears. It is usually an unknown quantity. To explore the effect of damping , the analysis was performed using a sequence of damping ratio values between 0.07 and 0.14. The analysis covered a range of rotating speeds at constant design load 2000 lb/in for both high-contact-ratio gears (HCRG) and low-contact-ratio gears (LCRG). The range of speed studied was 2000 to 12,000 rpm. The number of teeth 32, the diametral pitch 8, and the face width 1 inch were chosen for the basic dimensions of these gears. The results are shown in Figures IV.1 and IV.2 and Figures IV.3 and IV.4, for dynamic load factor and dynamic stress factor, respectively. As illustrated in these figures, damping has a major influence on both dynamic load and stress factors when the operating speed is close to the critical speed, or one-half or one-third of critical speed. Damping has little influence at other speeds. A large damping coefficient will reduce the dynamic motion at peak resonance speeds. This can be observed in Figures IV.1 through IV.4 for both low and high contact ratio gears.

The dynamic factor plots show that dynamic load factors of LCRG are much more speed sensitive than those of HCRG - especially if the damping is low. Also, the dynamic stress factors of HCRG are generally much greater than the dynamic load factors. These phenomena are influenced by the magnitude of the maximum dynamic load and its position. A small dynamic load near the tooth tip may produce a higher dynamic stress than that produced by a larger dynamic

49
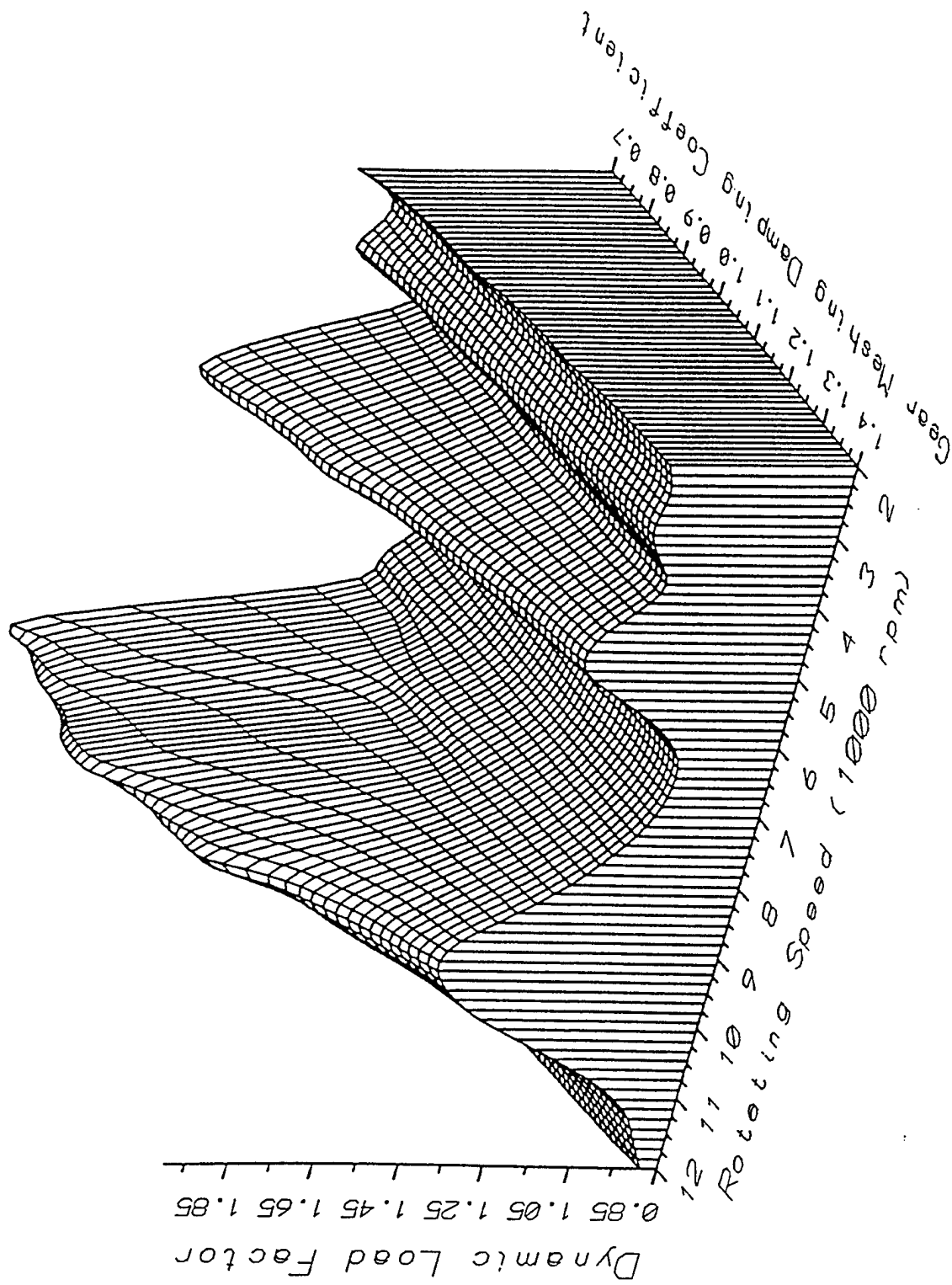
Figure IV.1 Three dimensional plot of dynamic load factor with variation of speed and damping for the sample low-contact-ratio gears

50
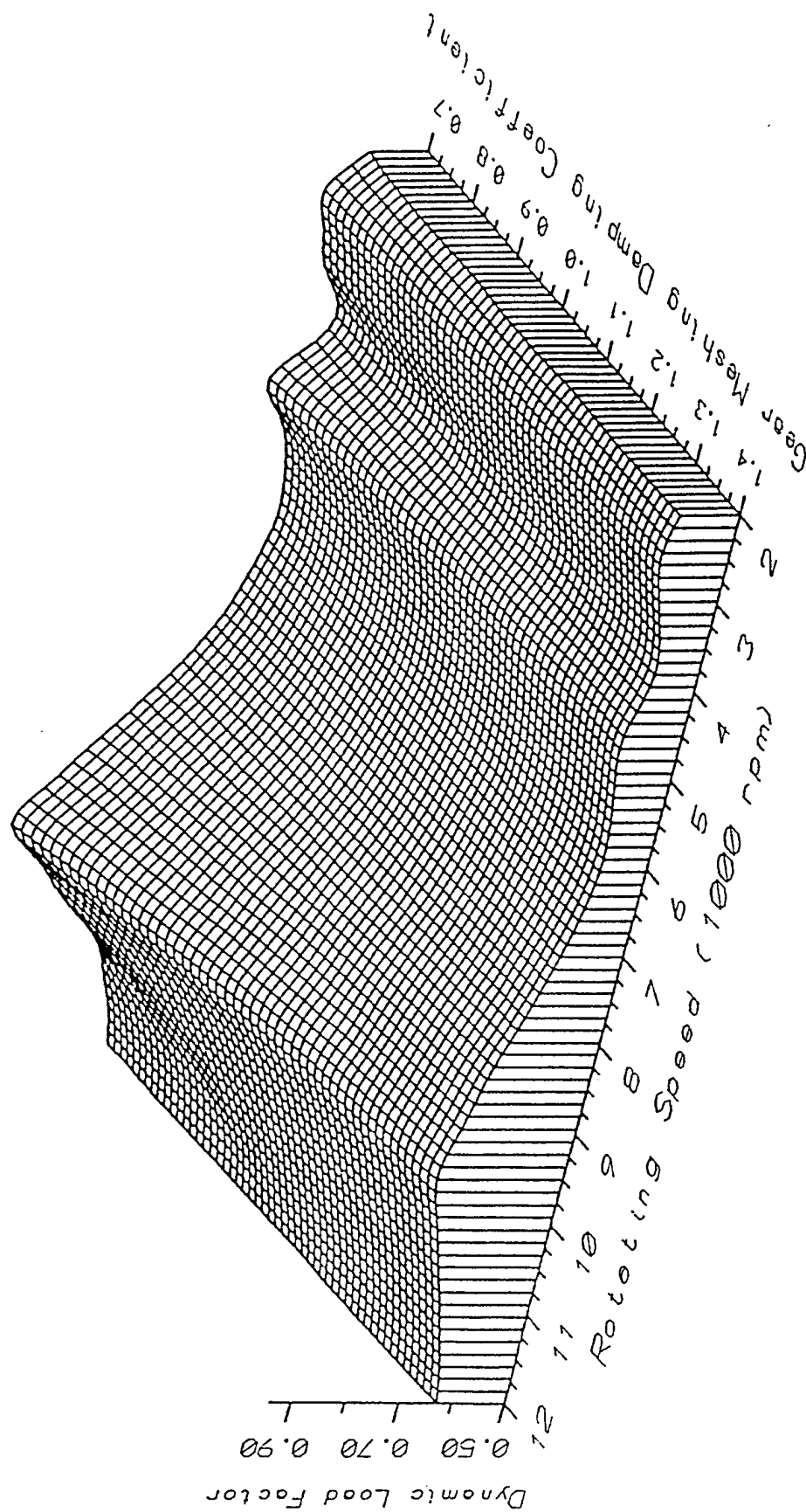
Figure IV.2   Three dimensional plot of dynamic load factor with variation of speed and damping for the sample high-contact-ratio gears

51
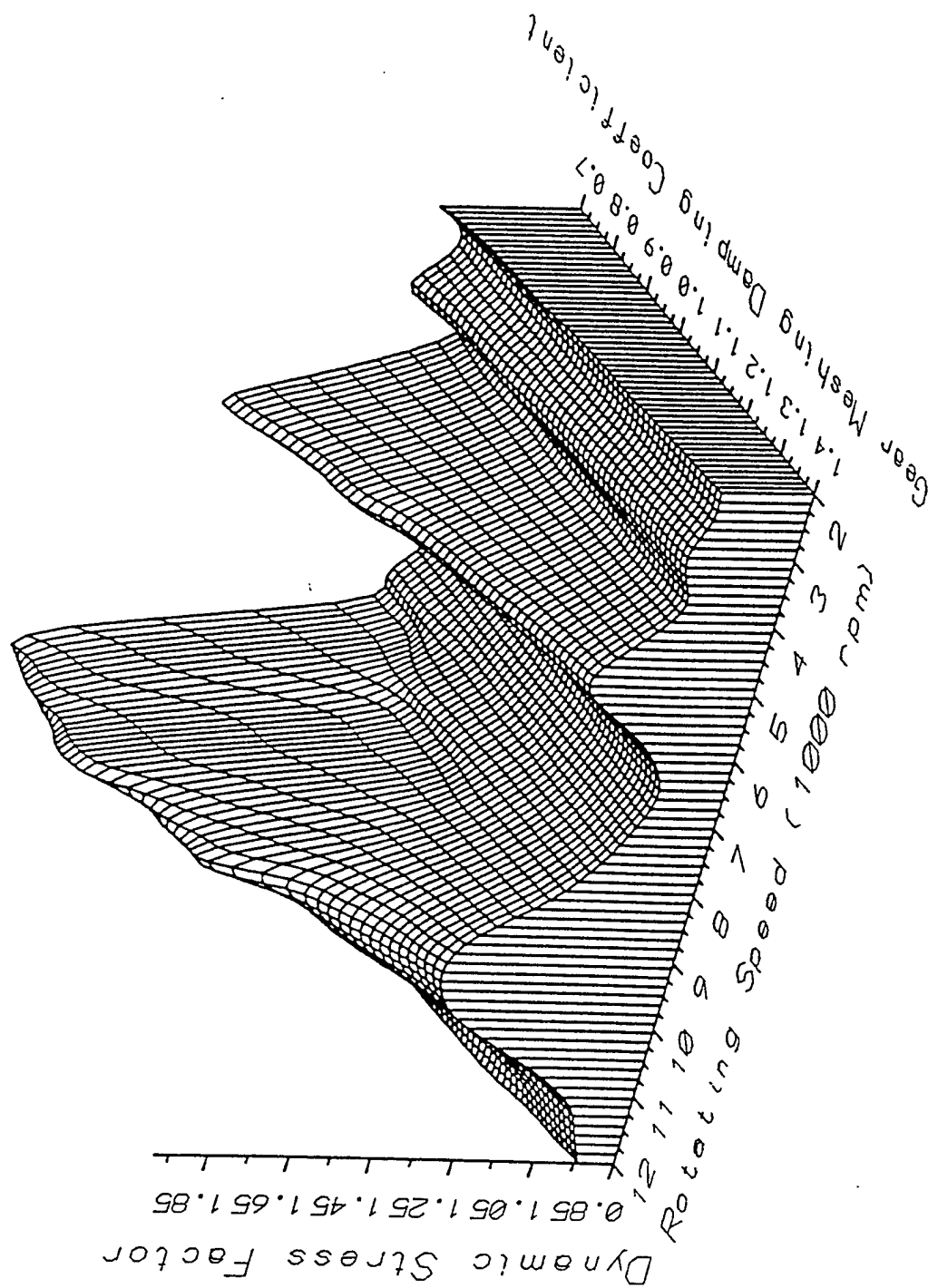
Figure IV.3 Three dimensional plot of dynamic Stress factor with variation of speed and damping for the sample low-contact-ratio gears
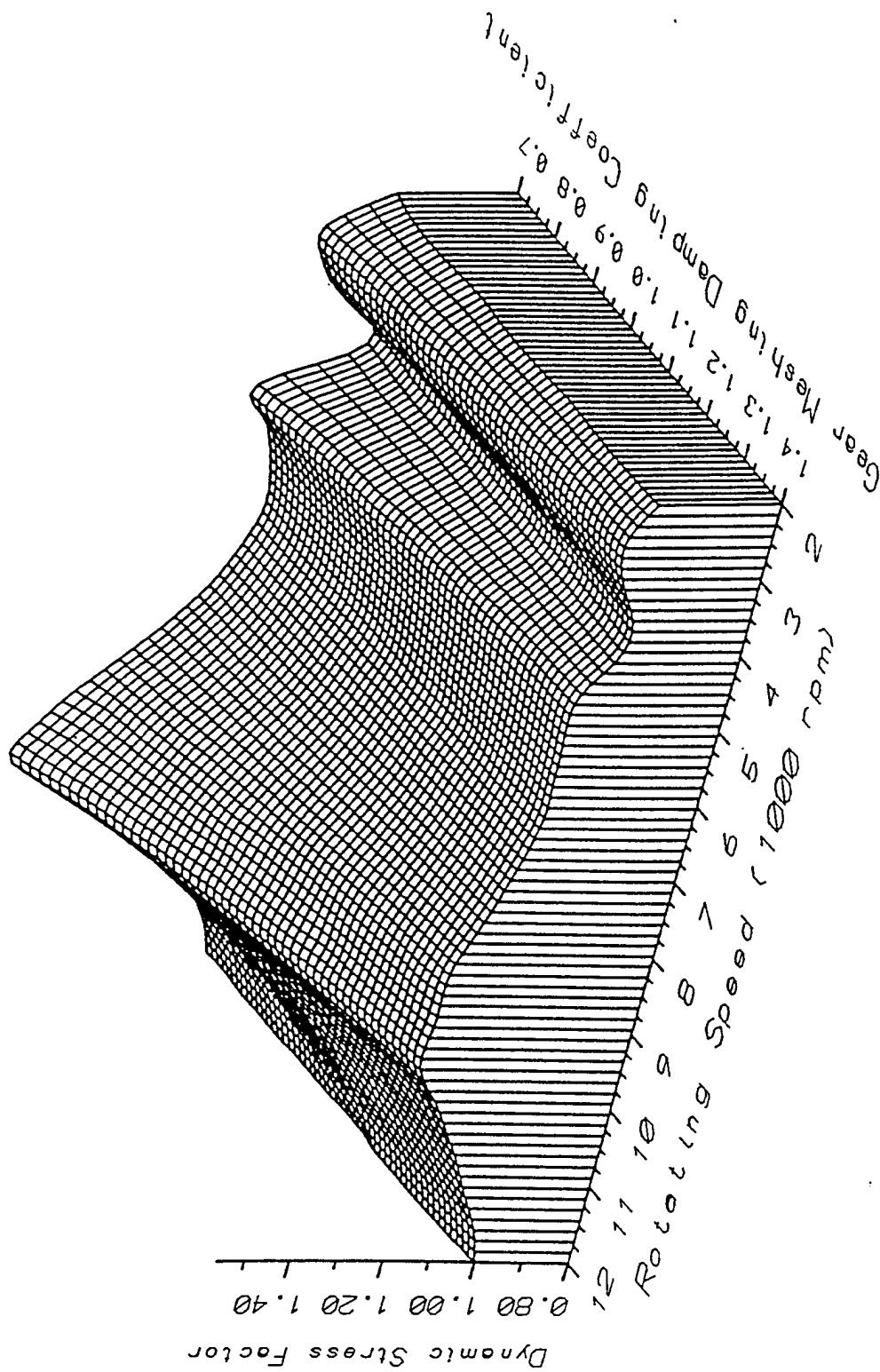
Figure IV.4 Three dimensional plot of dynamic stress factor with variation of speed and damping for the sample high-contact-ratio gears

load near the tooth root. Furthermore, a HCRG has a long, thin tooth which can produce a high stress at the fillet region.

Figures IV.5(a) and IV.5(b), which are static and dynamic load distribution plots for LCRG and HCRG, respectively, demonstrate the effect of different damping coefficients at resonance speed. The points of the curves where the dynamic load drops to zero indicate where the teeth lose contact during mesh, and the second peak of dynamic load occurs at the teeth re-engagement position. Figure IV.6(a) shows that the teeth separate when LCRG operate at resonance speed for all damping cases. There is no load exerted on the tooth and the value of tooth deflection is zero during the separation period. The average tooth stiffness for the entire tooth engagement period in this case is smaller than it would be if the teeth did not separate. This effect decreases the calculated value of the resonance speed.

Figure IV.6 shows the dynamic load and stress factors versus gear mesh damping coefficient for both HCRG and LCRG at resonance and sub-resonance speeds. For HCRG, the value of dynamic factors decreases smoothly as the gear mesh damping coefficient increases. This is also true for LCRG at sub-resonance speeds, but not for LCRG at resonance speed. For low contact ratio gears, resonance speed represents an unstable operating condition. In Fig IV.6 (a), there is a large change in the dynamic load factor at the damping coefficient value of 0.113. To understand this phenomenon, it is useful to look at the tooth static and dynamic load distribution plot (Figure IV.6) again. It can be observed that the teeth ar e out of contact longer for lower values of the damping coefficient. Since the gear meshing stiffness becomes zero when teeth lose contact, the average meshing stiffness becomes small and the resonance location shifts to a lower rotating speed. Since the damping coefficient cannot be directly controlled by a gear designer, we can reduce the risk of gear failure by avoiding the resonance region.

54
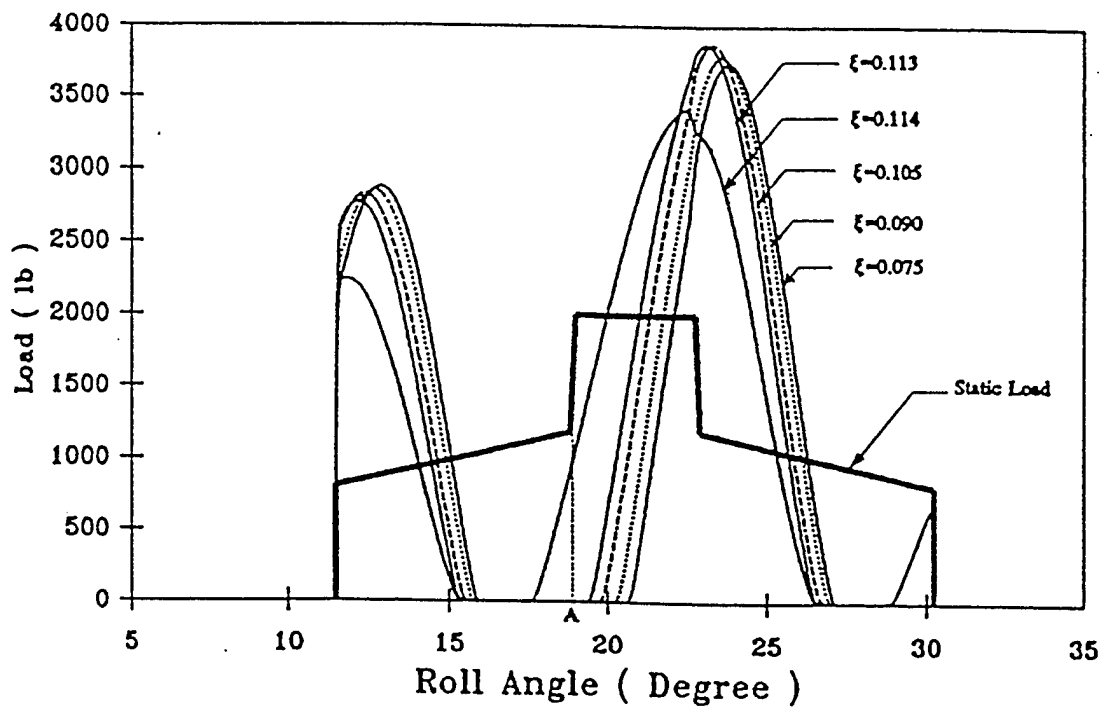
Figure IV. 5(a) Shared tooth load for sample LCRG pairs with various gear
mesh damping coefficient
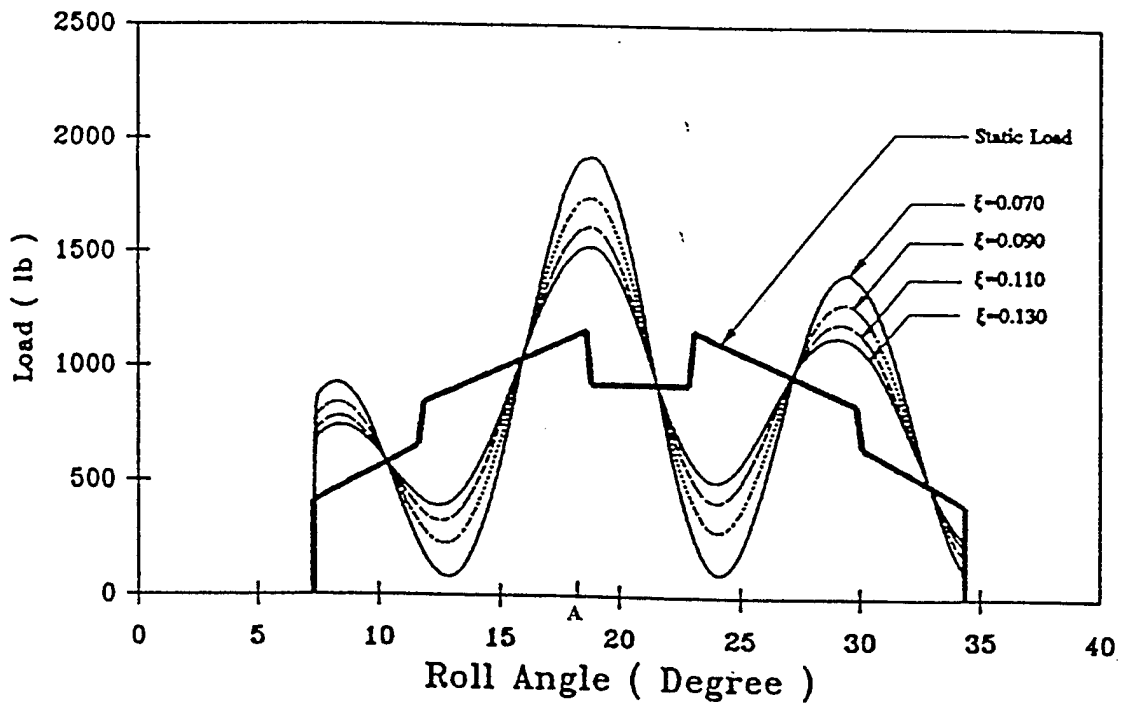
Figure IV. 5(b) Shared tooth load for sample HCRG pairs with various gear
mesh damping coefficient
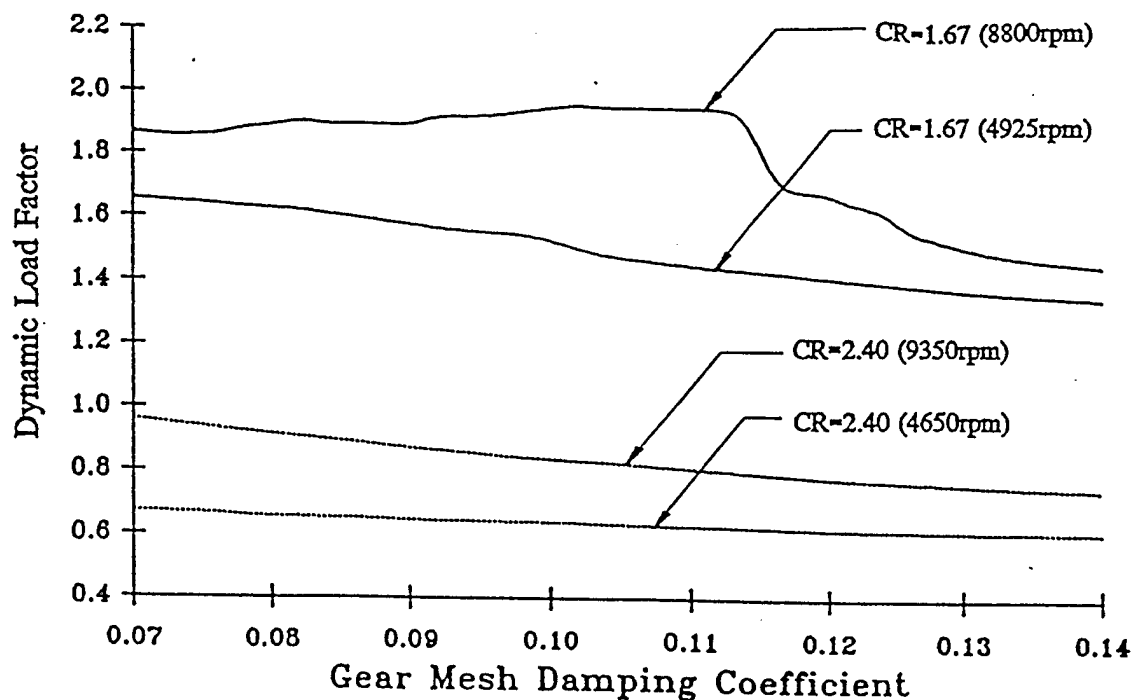
Figure IV. 6(a) Dynamic load factors versus gear mesh damping coefficient
for different contact ratio gears
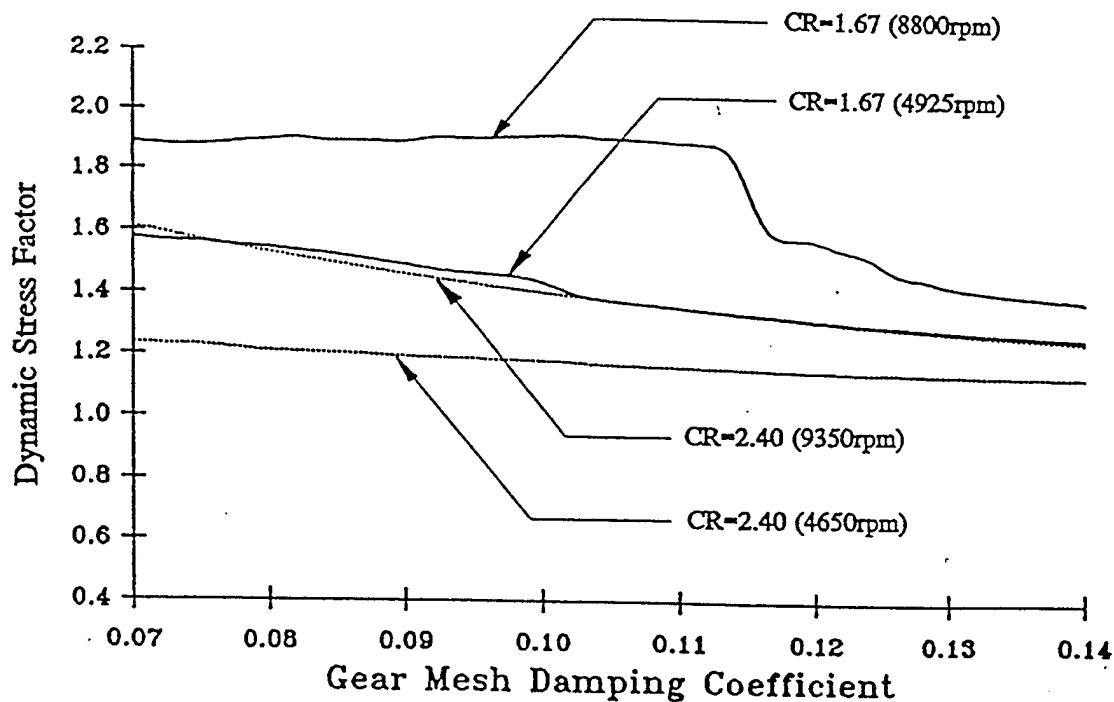
Figure IV. 6(b) Dynamic stress factors versus gear mesh damping coefficient
for different contact ratio gears

In most of the curves in Figure IV.6(a), tooth re-engagement occurs at around the tooth pitch point (roll angle = 20.854 degree) where the friction force reverses its direction. This causes the frictional torque around the tooth pitch point to change very sharply, producing unstable dynamic effects. For $\xi_g = 0.113$ and 0.114, the re-engagement points are located on either side of the point A (roll angle = 18.984) which is the transition point of double and single teeth contact area. In Fig IV.6(b) for HCRG, all the peak dynamic loads occur at the same position and there is no complete tooth separation for any damping case. The value of the maximum dynamic load is less influenced by ξ_g than with LCRG.

IV.2 Effect of Flexible Shaft and Bearing

Many gear dynamic models are based on the assumptions of rigid shafts and rigid rolling bearings. Rotor dynamics studies examine effects of the flexibility of the shaft and the mass unbalance of a gear body. The dynamic behavior of the gear system is affected not only by the tooth mesh stiffness but also by the elasticity of shafts and the rolling element bearings. The deflection of these supporting elements result in the deviation of the center of rotation from its original location. Hence, in order to obtain a more accurate prediction of the dynamic behavior of the overall gear system, the flexibility effects of shafts and bearings should be considered. These effects can be added to assembly misalignment. For the purpose of static analysis, it is sufficient to consider only relative radial motion of the center of gear rotation. The axial motion due to the shaft bending moment is negligible. A change of the center distance of a pair of gears will affect the pressure angle and the contact ratio. A detailed discussion of contact ratio effects will be illustrated in a later section.

Two typical rolling bearing-shaft systems are considered in this study. One has a gear mounted on a shaft between two bearings as in a simply supported beam, and the other has a gear

mounted on a shaft outside two supported bearings as in a cantilever beam. It is assumed that the materials of the gears and the shafts are homogeneous steel and there are no geometric errors in any of the components, therefore no eccentricity is considered. The flexural displacement of a rolling bearing due to the transmitted load can be divided into axial and radial direction components. Only the displacement in the radial direction affects the gear contact ratio. The outside diameter 1.5 inches and modulus of elasticity 30,000,000 psi were chosen for both shafts.

The computed results of the deflection due to a normal gear tooth load between 500 lbs and 2000 lbs are shown in Figure IV.7, and Figure IV.8(a) and (b) for simply supported beam and cantilever beam, respectively. Four types of the bearings were considered, type-1: deep-groove bearing, type-2: self-aligning bearing, type-3: spherical roller bearing, and type-4: tapered roller bearing. All of these have the same number (21) of rolling elements and 0.25 inch radius elements. The effective length 0.25 inch is chosen for the roller element and zero contact angle is selected for all the bearings. Since rolling elements in a ball bearing make point contact with the race way , the Hertzian contact deformation of a ball bearing is higher than in a roller bearing which has line contact. Thus, the deformation of the ball bearing is greater than that of the roller bearing. This can be seen in Figures IV.7 and IV.8, the deformations of both type-1 and type-2 bearings are larger than the deformations of type-3 and type-4, and they have a higher slope. The type-2, self-aligning bearing, is designed for moderate thrust force and can only resist a light radial load, thus has the maximum deformation. In the two cases shown, the shafts are relatively long, hence, the shaft deflections are much higher than the bearing deformations, especially with heavy loads. The change of a gear pair's center distance is governed by the shaft deflection. But, in the cantilever shaft case shown in Figure IV.8(b), the load exerted on bearing-2 is equal to the transmitted load plus the magnitude of the reacting load on bearing-1. This load produces the deformation of type-1 and type-2 bearings at the bearing-2 position as great as

58
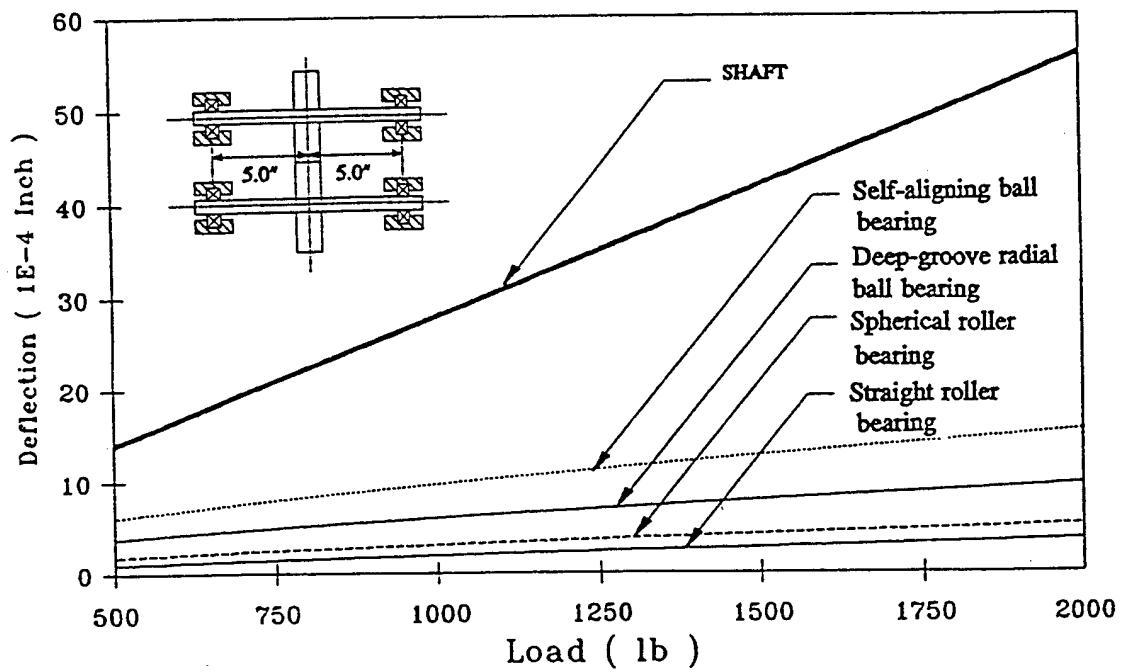
Figure IV.7 **Deflections of shaft and bearings under various loads for a simple two-bear-shaft system measured at gear position**
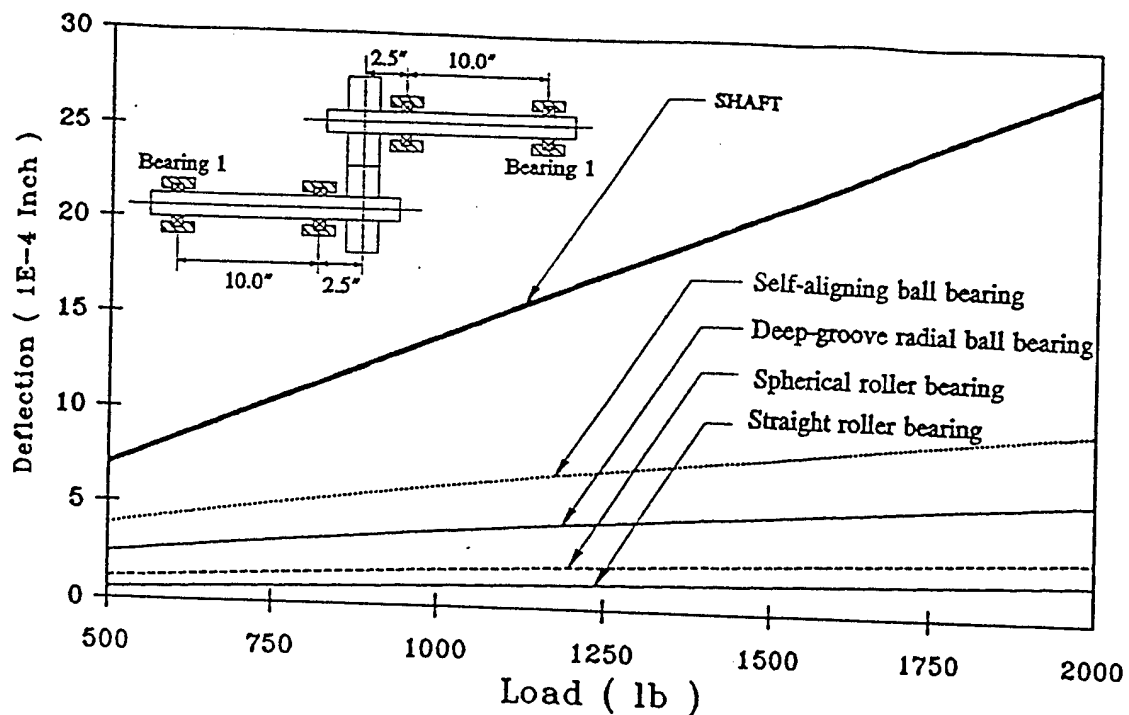
Figure IV.8(a) Deflections of shaft and bearings (at bearing-1) under various loads for a simple two-bear-shaft system, overhung load
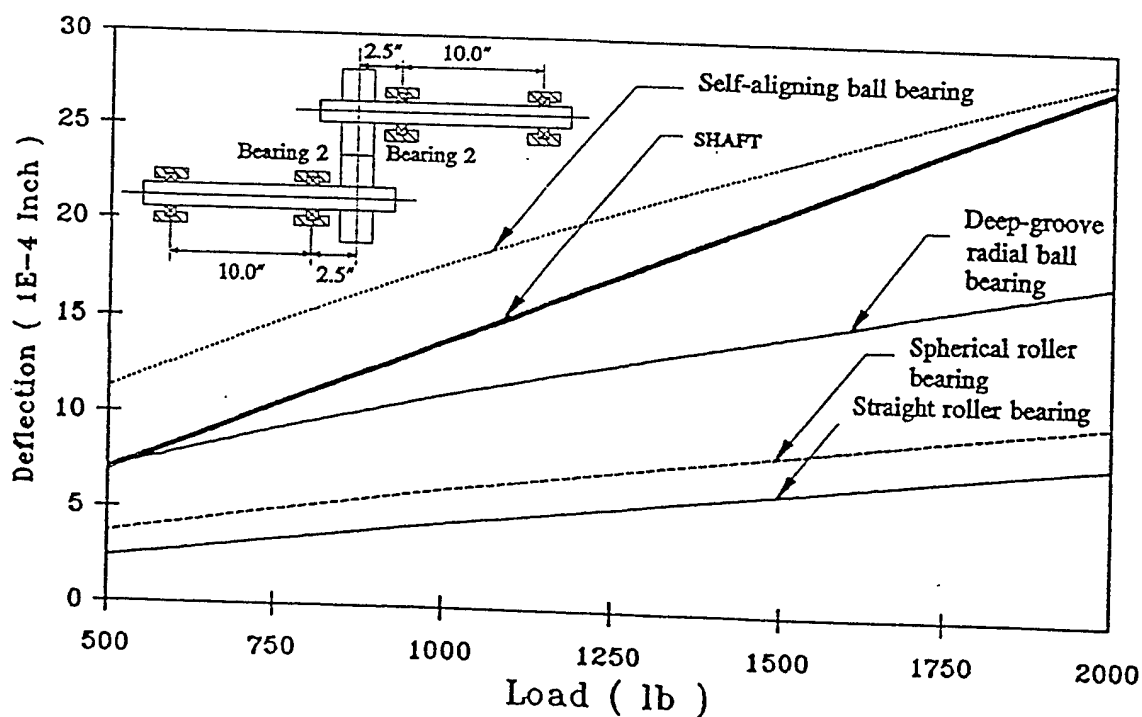

Figure IV.8(b) Deflections of shaft and bearings (at bearing-2) under various loads for a simple two-bear-shaft system, overhung load

the shaft deflection or even higher. In order to prevent failure a roller bearing or duplex ball bearings may be needed in the bearing-2 position.

Figures IV.9 and IV.10 show the resulting change in contact ratio due to combined deflection at various gear mounting positions. In the simply supported shaft case, Figure IV.9, the maximum deflection occurs when both gears are mounted at the center of the shafts. This causes the minimum contact ratio. In the cantilever shaft case, Figure IV.10, increasing the overhang of the gears reduces the contact ratio. Gear shaft deflection, especially for overhung gears, also creates misalignment which can lead to edge contact of the gear teeth.

The contact ratio is influenced by the center distance: increasing the center distance reduces the contact ratio. This is illustrated in Fig IV.11 which compares the effect for gear sets of two different sizes and both standard addendum. For the two larger gear sets (diametral pitch 8 and 32 teeth) the curves for contact ratio vs. increase in center distance have the same slope. For the smaller gear sets (diametral pitch 12 and 32 teeth) the slopes of the curves are equal to each other but steeper than the curves for the larger 8 pitch gears. This demonstrates (1) the sensitivity of contact ratio to center distance is not affected by the tooth addendum and (2) smaller gears with smaller teeth are more sensitive to center distance variation.

IV.3 Effect of Contact Ratio

The contact ratio is defined as average number of tooth pair(s) in contact. It may also be defined as the ratio of the length of contact for one tooth pair to the base pitch. The contact ratio is a key parameter for dynamic behavior of gears.

The contact length is measured on the line of action between the initial contact point and the end contact point. In general, the higher the contact ratio, the longer the overlap where more than one pair of teeth are in contact, and the more smoothly the gears will run. It is possible to increase the contact ratio to greater than two by carefully manipulating the gear design

61
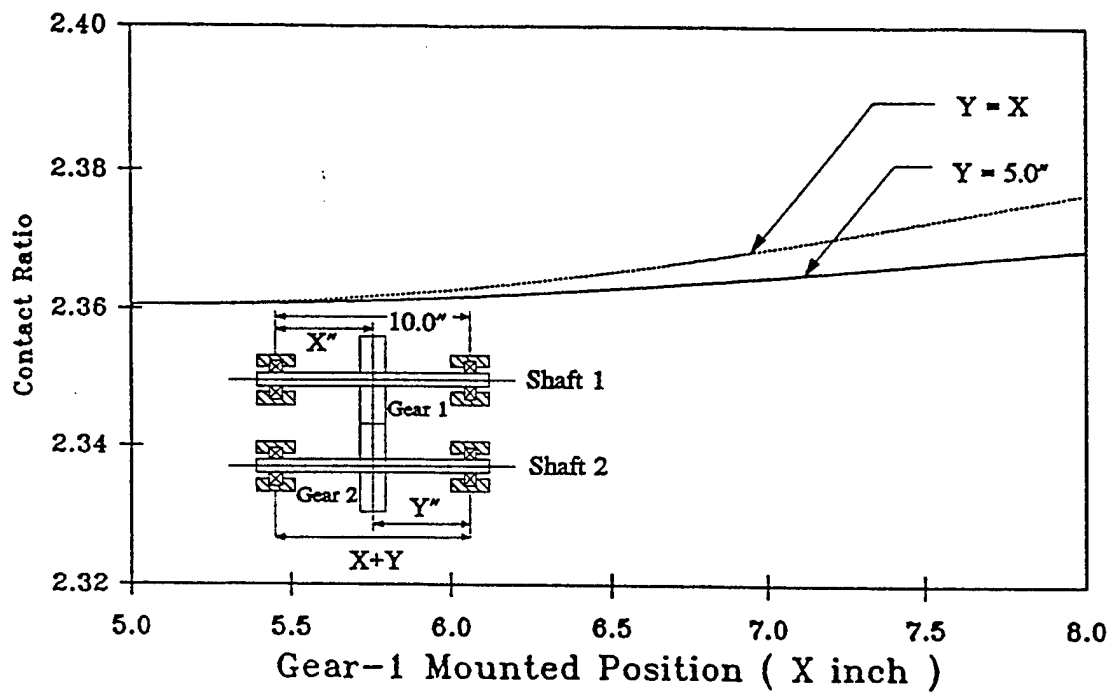
Figure IV.9 Effect of gear mounting position in a simple two-bearing-shaft system
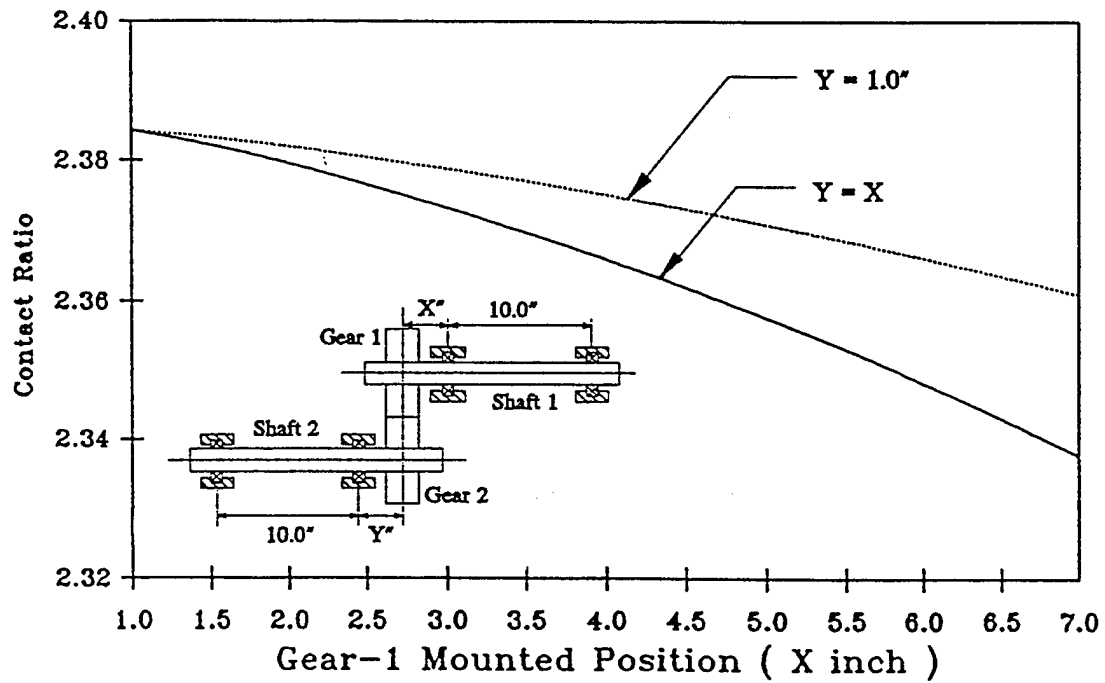
Figure IV.10 Effect of gear mounting position in a simple two-bearing-shaft system, overhung load
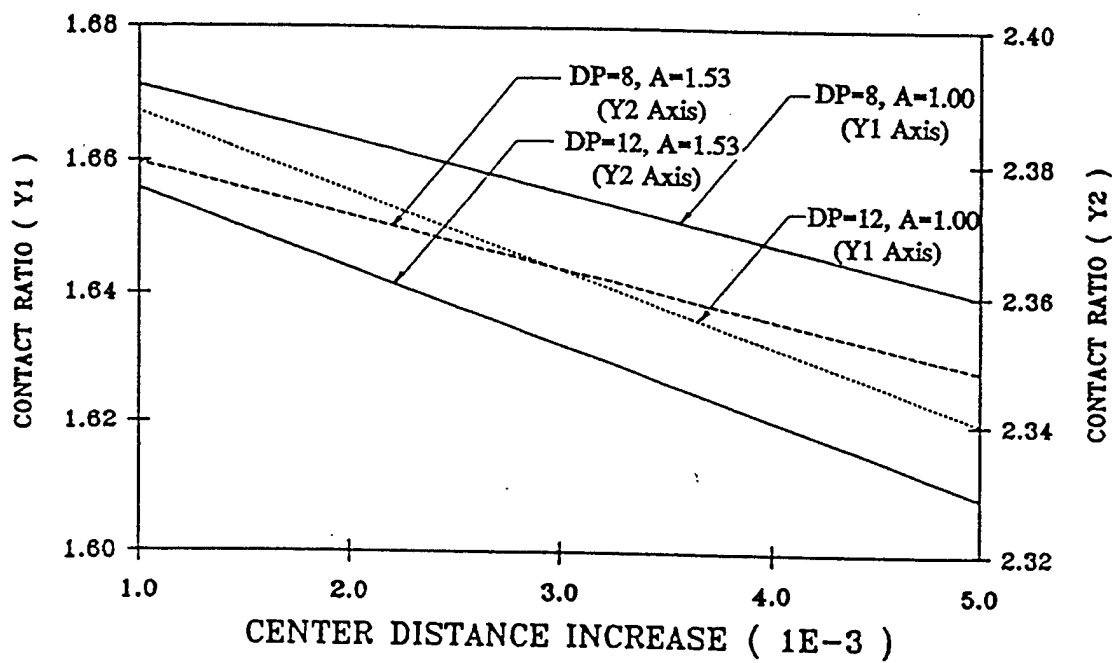
Figure IV.11   Effect of increase in center distance for sample LCRG and HCRG
pairs (All gears have 32 teeth)

parameters. Figures IV.12(a) and (b) illustrate how an increase in the normalized tooth addendum A from 1.0 to 1.4 raises the contact ratio from 1.26 to 2.46.

Although it is beneficial to distribute the load among more pairs of teeth, the load capacity of a gear set may suffer due to longer moment arm as a result of going to a higher contact ratio. Therefore, gear design represents a compromise between various design requirements. Furthermore, in order to operate HCRG effectively, the gears have to be manufactured to a higher degree of precision so that the load can be properly shared by the three or more pairs of teeth in contact.

High contact ratio gears can be designed in several ways: (1) by selecting a greater value of diametral pitch (smaller teeth), (2) by increasing the length of tooth addendum, and (3) by choosing a smaller pressure angle. Those parameters can be changed individually or in combination to achieve the desired contact ratio. Raising diametral pitch increases the number of teeth and diminishes the tooth thickness, which will reduce the tooth strength. Augmenting the length of the addendum causes the tooth to become longer which increases the bending stress at the fillet region. A lower pressure angle increases the tangential force component acting on the tooth. This makes a higher bending moment. Moreover, it raises the chances of interference, and reduces the tooth thickness at the root. Generally speaking, high-contact-ratio gears tend to have weaker teeth. They also have a greater tooth sliding velocity which may produce higher surface temperatures and greater tendency for surface-distress-related failures. Increasing the tooth addendum is usually the preferred method to obtain high-contact-ratio gears because this can be done by adjusting the cutting depth during the manufacturing process.

This study investigates the effect of varying the contact ratio for a typical set of spur gears. Design parameters for the gears are shown in Table IV.1. The contact ratio is varied over the range 1.26 to 2.46 by increasing the normalized tooth addendum from 0.7 to 1.54. The results

65
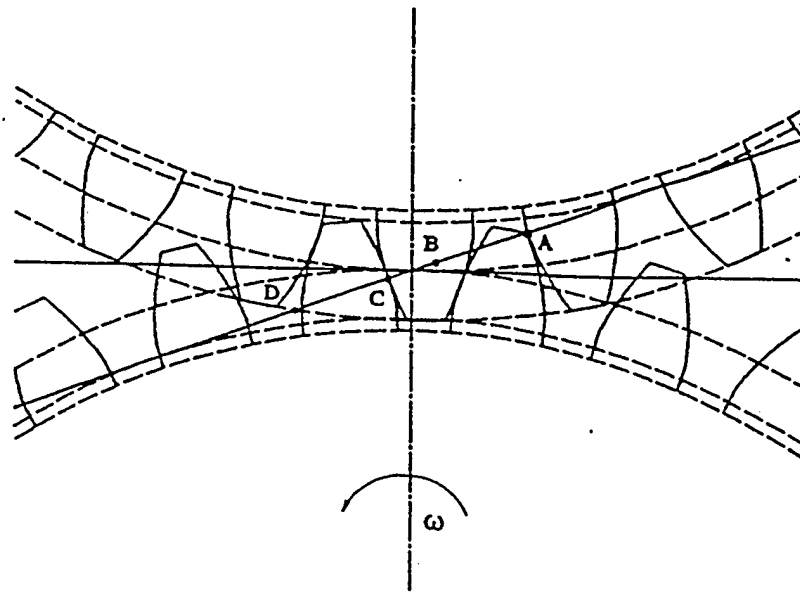
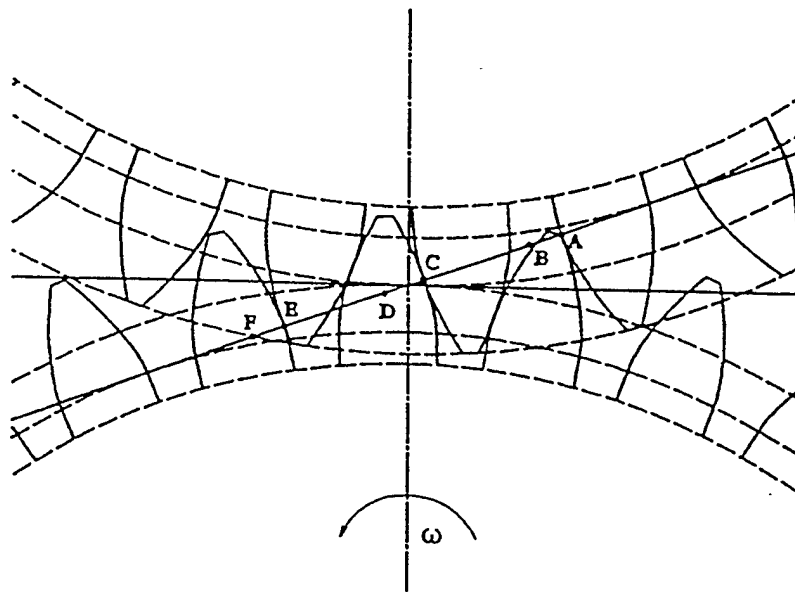Figure IV.12(a) Tooth contact in low-contact-ratio gear

Figure IV.12(b) Tooth contact in high-contact-ratio gear

are shown in the form of the dynamic load factor plotted as a function of rotating speed in Figure IV.13 for LCRG and Figure IV.14 for HCRG.

In Figure IV.13, for LCRG, the dynamic load factor generally decreases as the gear contact ratio increases. This phenomenon is most prominent at the main resonant speed, near 9000 rpm, and at one-half of this resonant speed. The gears with the highest contact ratio (CR = 1.868) have lower dynamic load at all speeds. We believe that this effect is due to the very narrow band of single-tooth contact being passed so quickly during gear rotation that the system could not respond until after the excitation has passed. The high speed behavior of LCRG with contact ratio close to 2.0 is similar to that of high-contact-ratio gears shown in the following figures.

In Figure IV.14, for HCRG, there is much less dynamic action; none of the dynamic load factors of HCRG exceed 0.9 even at resonant speed. Contrary to LCRG, the higher the contact ratio of HCRG the higher the dynamic factor in the resonance zone. The gears with the lowest contact ratio (CR = 2.226) have the highest dynamic load at lower speeds, but the trend reverses at the resonant speed where the gears with the highest contact ratio experienced the highest load. This phenomenon may be due to excitation from the transition between double- and triple-tooth contact. For gears with contact ratio equal to 2.226 the triple-tooth-contact region is shorter than that of the other two cases with high contact ratios. The excitation due to the change in number of teeth in contact(which changes the meshing stiffness) acts like a short-duration impulse, which is more effective at lower speeds than at higher speeds.

Figure IV.15 compares the dynamics of "transition" gears from LCRG to HCRG (CR = 1.952, 2.000, and 2.145). The dynamic curves for CR = 1.952 shows a trend similar to that for CR = 1.868 in Figure IV.13. For gears with a contact ratio of exactly 2.0, there is almost no variation of the meshing stiffness during tooth contact. As a result the dynamic response is very

67

Table IV.1   Sample Gear Parameters

Pressure Angle (degree)	20.0
Diametral Pitch (DP)	8
Number of Teeth	32
Addendum, (normalized by 1/DP in.)	0.7 ~ 1.45
Backlash (in.)	0.001
Pitch Diameter (in.)	4.0
Outside Diameter (in.)	4.175 ~ 4.385
Root Diameter (in.)	3.775 ~ 3.565
Face Width (in.)	1.0
Design Torque (lb-in.)	3760
Static Tooth Load (lb/in.)	2000
Tooth profile	involute
Damping ratio	0.10
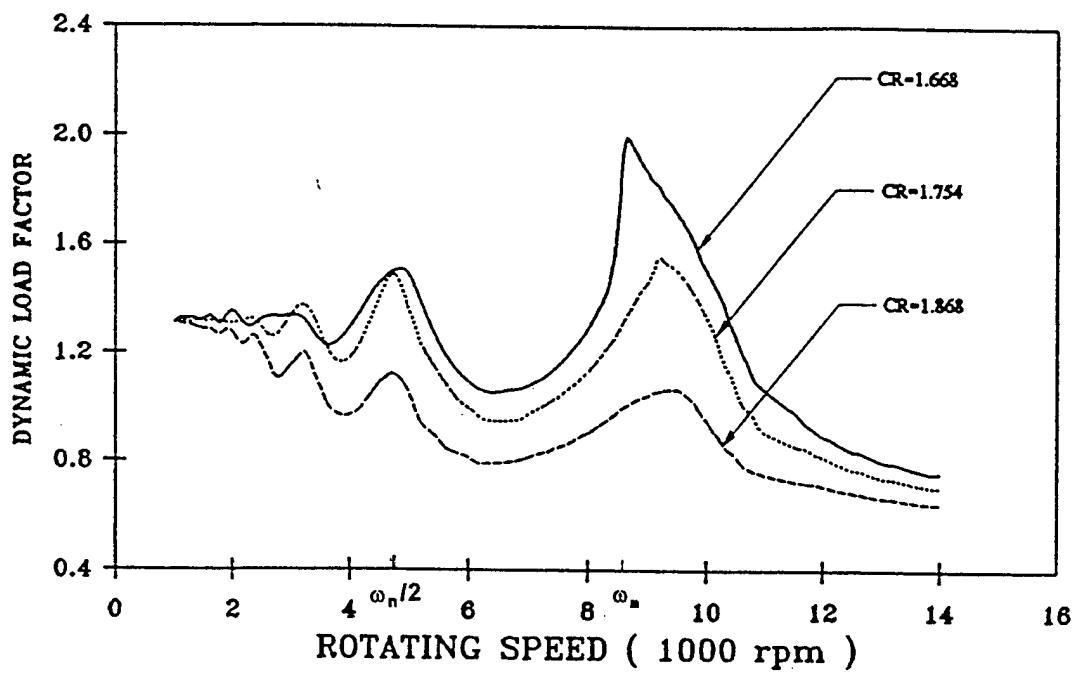
Figure IV.13 Dynamic load factor versus rotating speed for LCRG
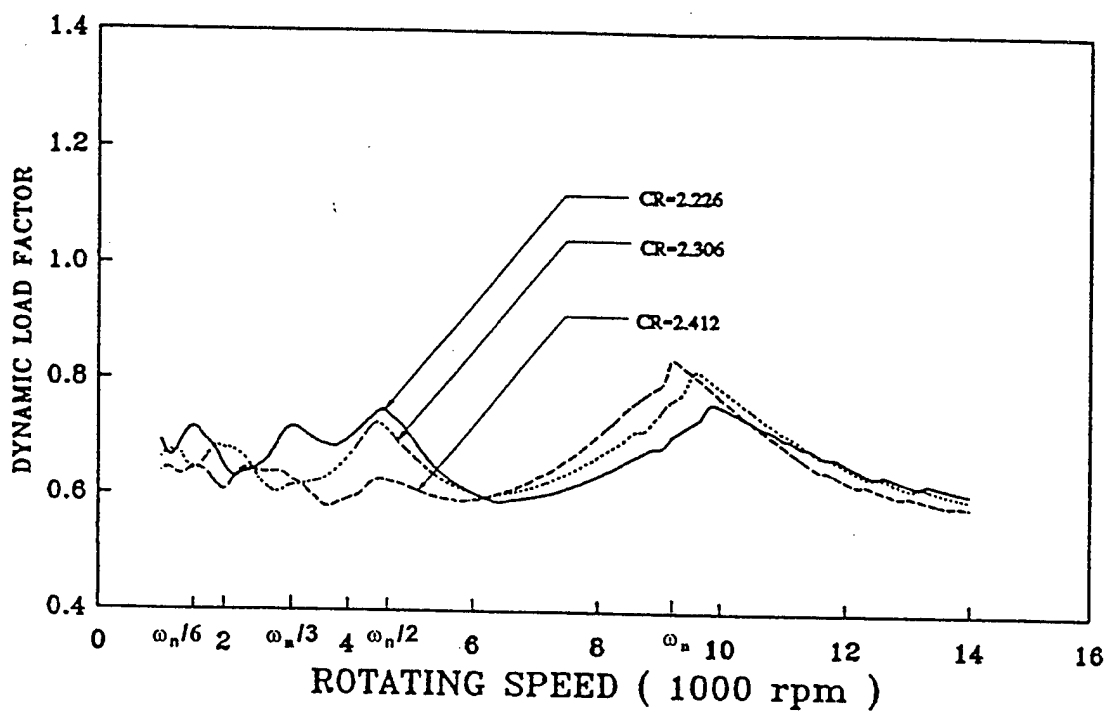
Figure IV.14 Dynamic load factor versus rotating speed for HCRG
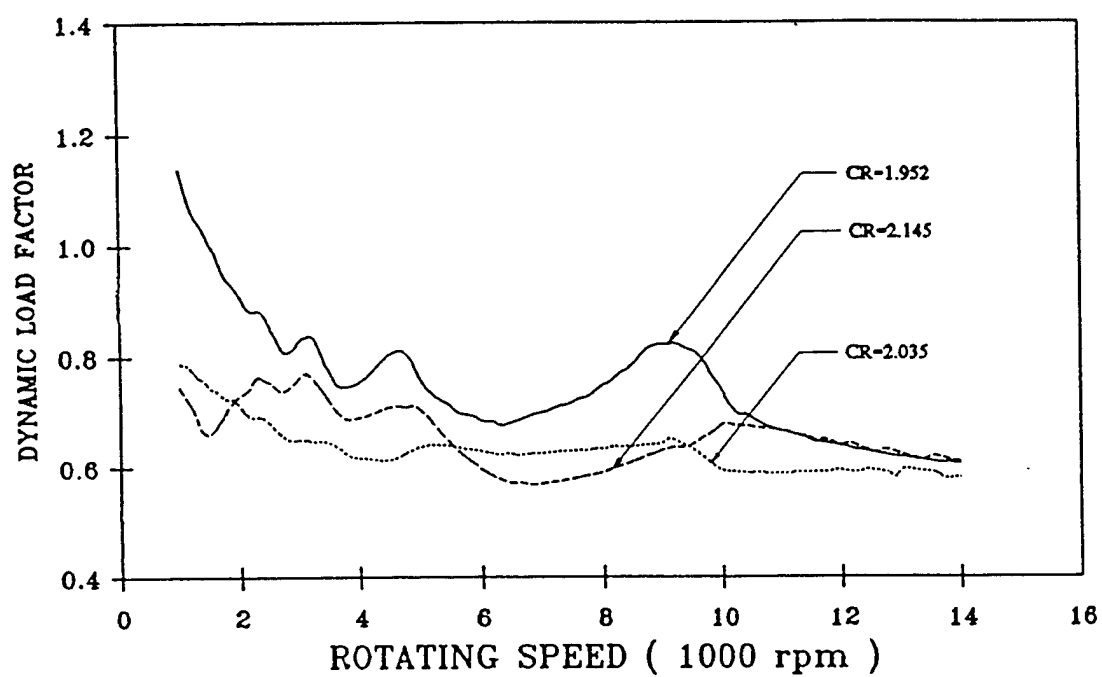
Figure IV.15 Dynamic load factor versus rotating speed for the gear pair
with CR near 2.0

gentle, even at resonant speeds. At CR = 2.145 excitation due to the meshing stiffness variation between double- and triple-tooth contact produced some dynamic effect at lower speeds (below 5000 rpm). As speed increased beyond 5000 rpm, the effect of stiffness variation diminished, as shown in the figure.

The effect of varying contact ratio (CR) on the dynamic load factor and dynamic stress factor at the critical speed (ω_n) and certain submultiples of this speed are shown in Figures IV.16 and IV.17. 9300 rpm is the first critical speed for tooth mesh excitation, and 4650 rpm is one-half of this speed. The data in Figure IV.16 may be grouped into three zones: In zone 1, where contact ratio is less than 1.7, the dynamic load factor at critical speed is nearly constant at approximately 1.9. For the submultiples of the critical speed, the dynamic load factor oscillates around a level about 25 percent less than that of the critical speed. In zone 2, a transition zone where the contact ratio changes from approximately 1.70 to 2.0, the dynamic load factor drops rapidly as the contact ratio increases, reaching a minimum of 0.64 at CR = 2.0. The dynamic load for the critical speed falls off first, and then the smaller submultiples fell off at a higher contact ratio value. Finally, in zone 3, where the contact ratio is greater than 2.0, the dynamic load factor oscillates between 0.64 and approximately 0.8. As a general trend, dynamic loads for high contact ratio gears are smaller than for LCRG.

The dynamic tooth bending stress depends on the dynamic load and also the location on the tooth where this load occurs. A high load acting near the tooth tip causes higher bending stress than a similar load applied lower on the tooth. Figure IV.17 shows the variation of the dynamic stress factor with contact ratio at the critical speed (ω_n) and submultiples of ω_n. As in the previous discussion for dynamic load factor, in zone 1, (where the contact ratio is greater than 1.7), the dynamic stress factor at ω_n declines slightly from about 2.0 to 1.7 as the contact
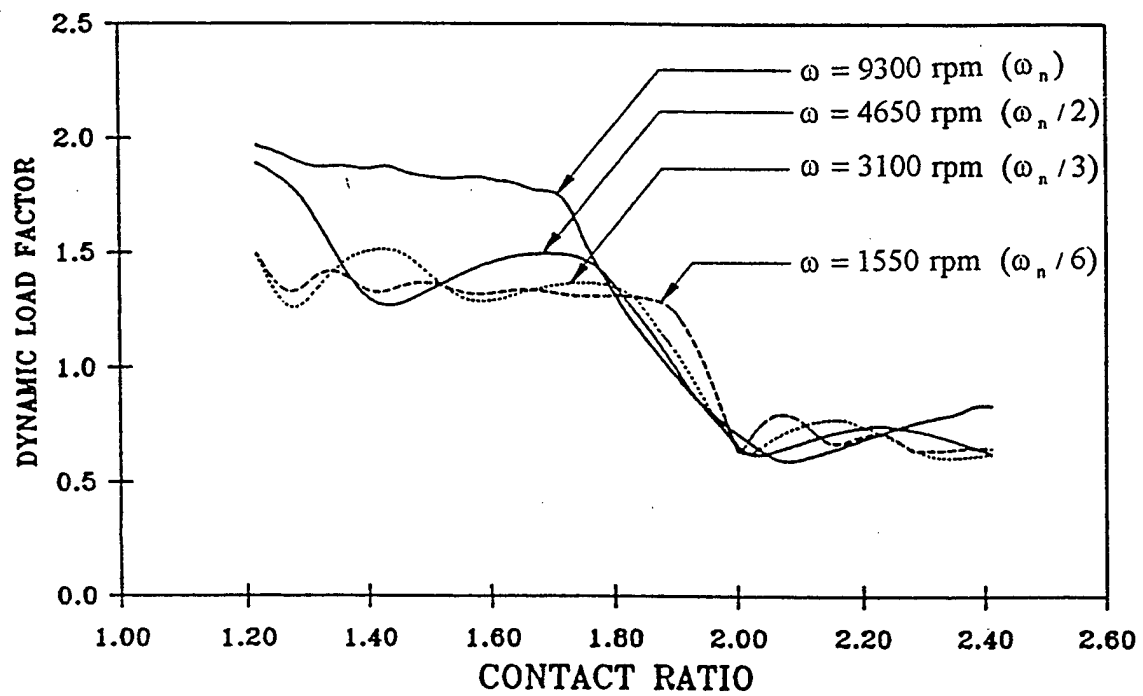
Figure IV.16 Dynamic load factor versus contact ratio at certain rotating
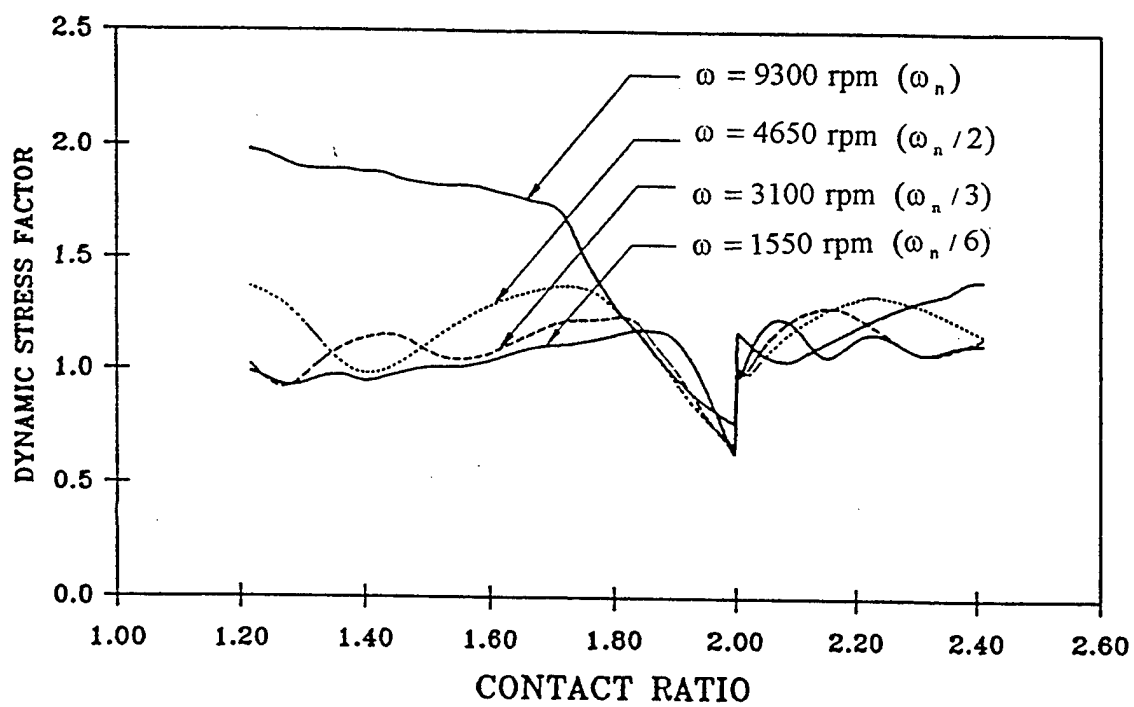speeds

Figure IV.17 Dynamic stress factor versus contact ratio at different rotating speeds

ratio increases slightly with contact ratio. In zone 2 (transition from low to high contact ratio), the dynamic stress factor declines significantly to a minimum value of 0.65 at CR=2.0. In zone 3, where the contact ratio is greater than 2.0, the dynamic stress oscillates between approximately 1.03 and 1.35. At the critical speed, the dynamic stress is much higher for LCRG than for HCRG, however, at submultiples of the critical speed, the dynamic stress factors for HCRG and LCRG are nearly equal. At all speeds, the dynamic stress factor is lowest for gears with CR=2.0.

Figures IV.16 and IV.17 show that increasing the contact ratio does not always reduce the dynamic load or dynamic stress. For gears that operate over a wide range of speeds a contact ratio close to 2.0 is the best choice. Although a high contact ratio gear (CR>2.0) may have a relatively low dynamic load factor, the dynamic stress may not be low because of the taller teeth.

A three dimensional representation of the effect of the speed and contact ratio on the dynamic load and dynamic stress factors are shown in Figures IV.18 and IV.19, respectively. The dynamic load and dynamic stress show similar trends when the contact ratio is smaller than 2.0. However, the dynamic stress factors are much higher than the dynamic load factors when the contact ratio is greater than 2.0. The corresponding contour diagrams in Figures IV.18(b) and IV.19(b) show that although the dynamic load is generally low throughout the entire HCRG region, the dynamic stress remains high. These contour diagrams are good tools for pinpointing the exact position of the dynamic peaks and valleys for a gear design. Gears with minimum dynamic load and stress will be located in the valleys of these diagrams. In Figures IV.18 and IV.19, dynamic load and dynamic stress factors are minimum near CR = 2.0.

For some applications it may not be feasible to design a gear system with a contact ratio of 2.0. Moreover, the contact ratio of a gear pair may be altered by shaft deflection. Figure IV.18 and IV.19 show the effects of such changes for the gear system analyzed in this report. An analysis code such as DANST can be used to generate similar data required for designing other gear systems.
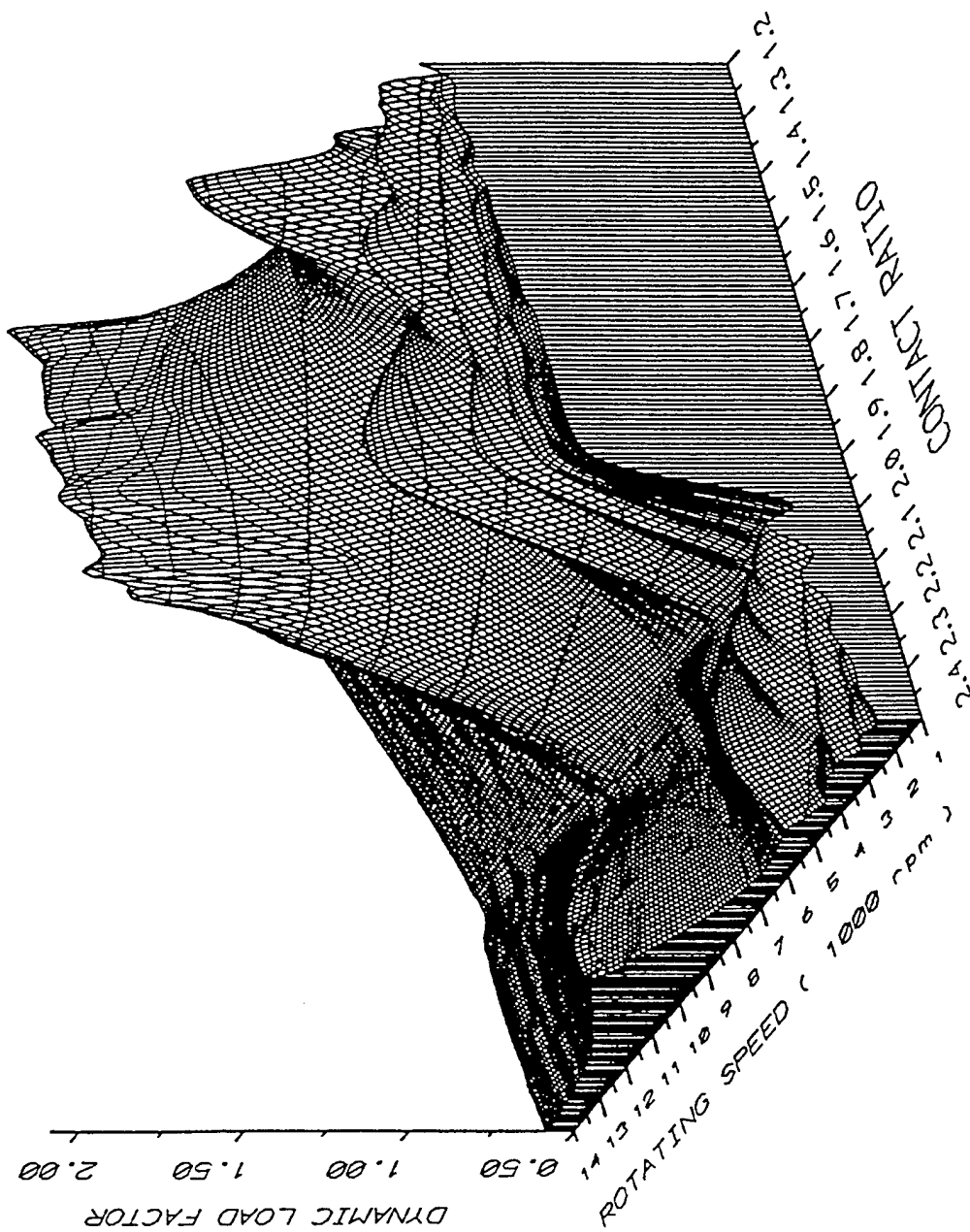
Figure IV.18(a) Three dimensional plot of dynamic load response with variation of speed and contact ratio for the sample gears
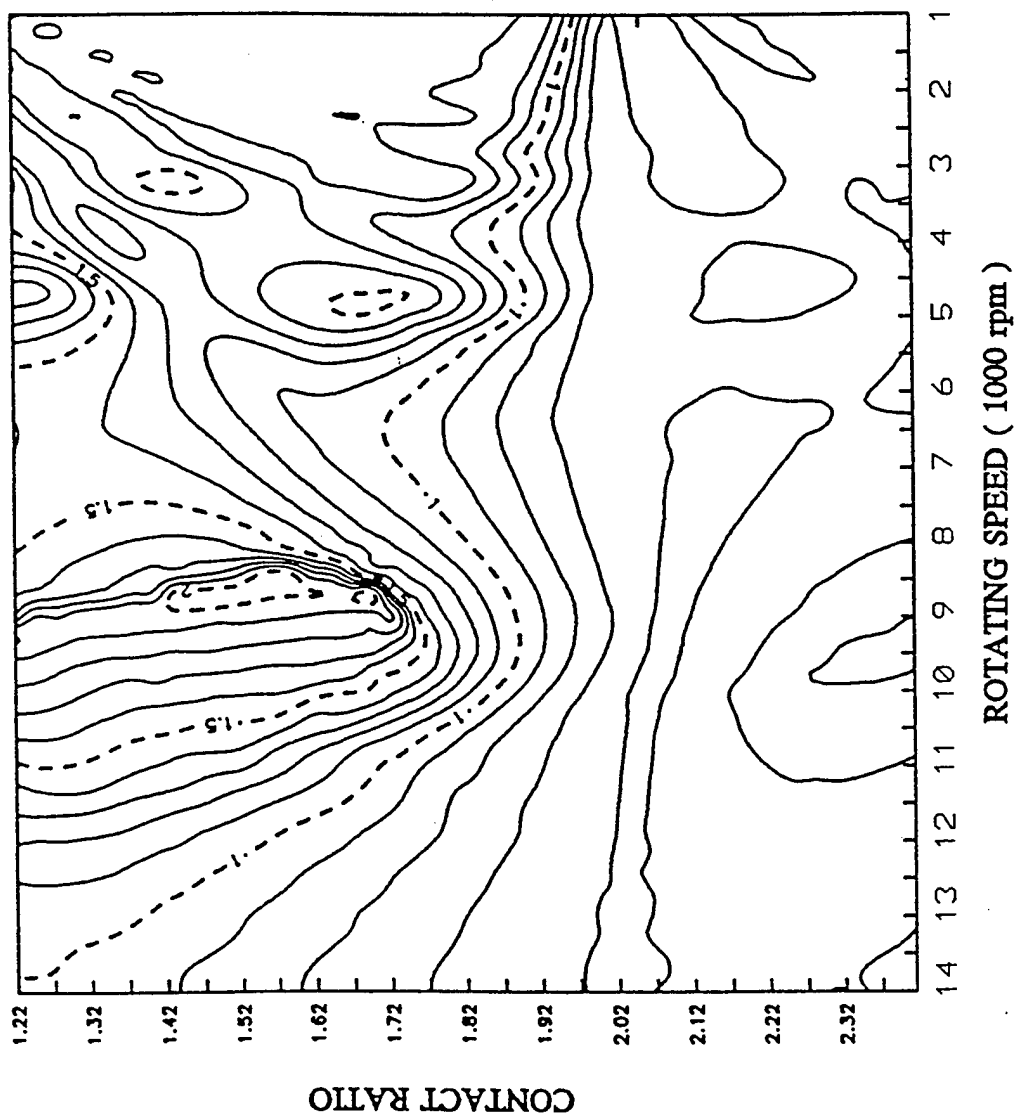
Figure IV.18(b) Contour plot of dynamic load response with variation of speed and contact ratio for the sample gears
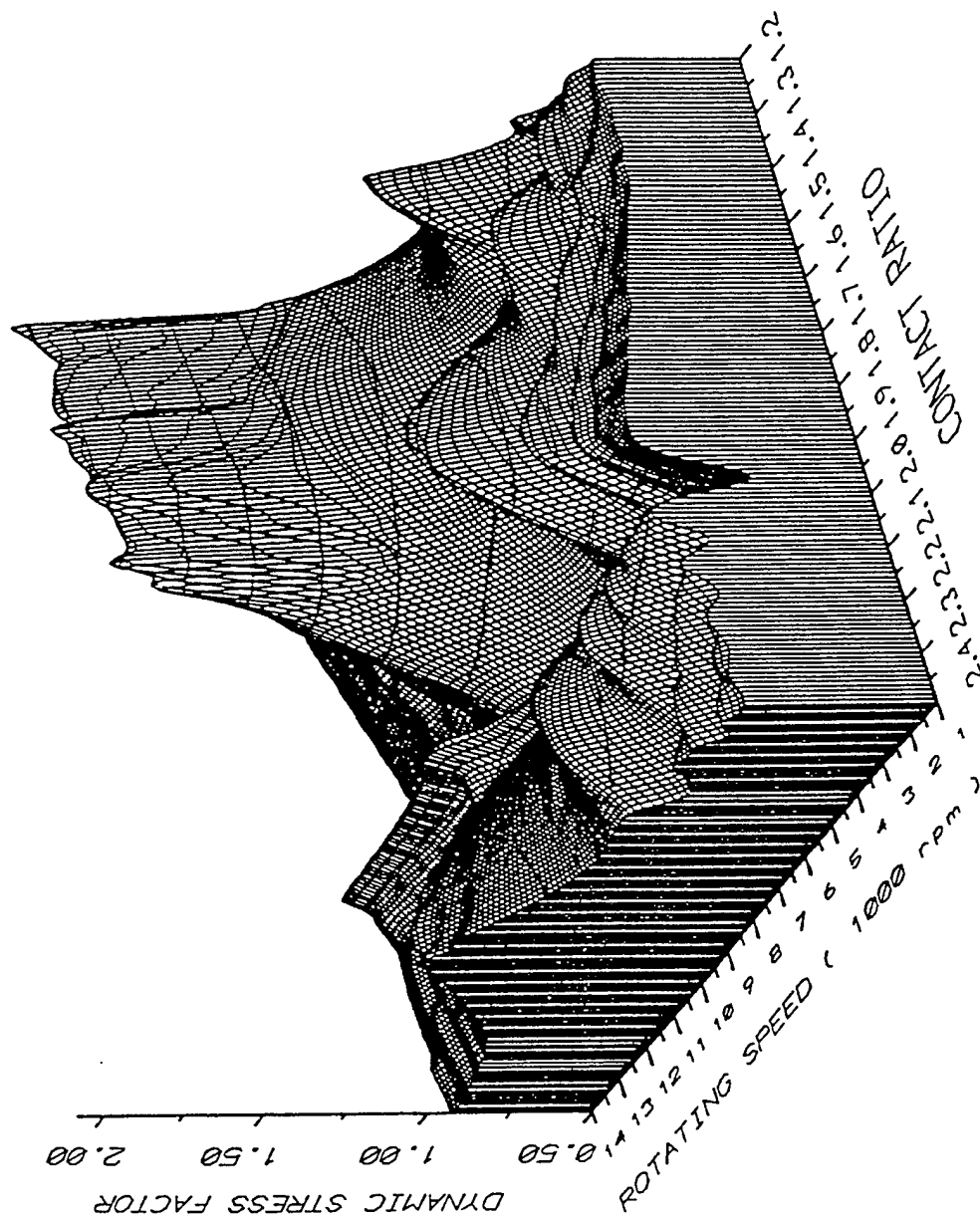
77

Figure IV.19(a) Three dimensional plot of dynamic stress response with variation of speed and contact ratio for the sample gears
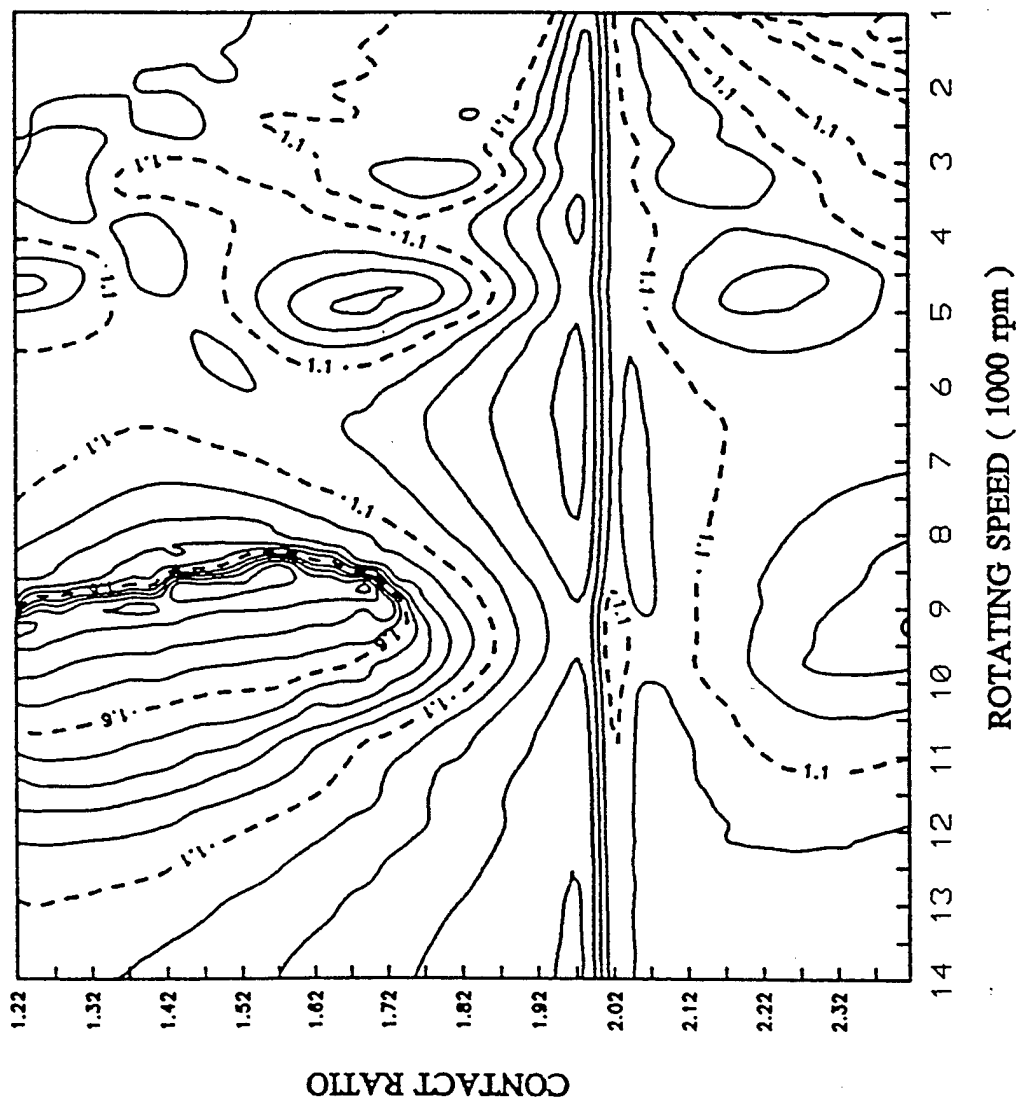
Figure IV.19(b) Contour plot of dynamic stress response with variation of speed and contact ratio for the sample gears

CHAPTER V

CONCLUSIONS

The flexibility effects of shafts and bearings have been added to previous work [13, 14] to improve the simulation of gear dynamics. Parametric studies of gear dynamic behavior were performed using the computer program DANST. A wide range of the gear mesh damping coefficient values, from 0.07 to 0.14, were examined to study the influence of the damping on gear dynamics. The effect of contact ratio on gear dynamics was investigated. Contact ratios ranging from 1.20 to 2.40 can be obtained by varying the length of the tooth addendum for a sample pair of spur gears used for the analysis. Other parameters which also affect the value of contact ratio were held constant in this study.

Based on the results from the analytical investigations, the following conclusions were obtained.

(1) Generally speaking, dynamic tooth bending stress in high-contact-ratio gears is higher than that in low-contact-ratio gears. When the contact ratio approaches 2.0 significantly lower dynamic stresses were found throughout the speed range.

(2) Damping has a major influence on dynamic response only when the operating speed is close to a resonant speed, and a much less influence when operating speed is near sub-multiple of the resonant speed.

(3) The contact ratio of a gear pair is influenced by the operating center distance. In order to determine actual contact ratio of gears in operation, gear designers should take the deflections of shafts and bearings into design consideration.

(4) Dynamic effect is significantly higher for low-contact-ratio gears than for high-contact-ratio gears. There is a benefit of using high-contact-ratio gears for minimizing gear dynamic load.

(5) In general, for low-contact-ratio-gears, increasing the contact ratio reduces dynamic load. The most significant effect occurs as the contact ratio approaches 2.0. Dynamic effects are minimized at contact ratios near two. For high-contact-ratio gears, the optimum contact ratio value depends on the operating speed. Increasing contact ratio does not always reduce dynamic load.

(6) At very high speeds (above the critical speed), the dynamic response of a gear system is much less influenced by the contact ratio or by small speed changes.

BIBLIOGRAPHY

[1] Buckingham E., "Dynamic Load on Gear Teeth", Report of Special Research Committee on the Strength of Gear Teeth, ASME, New York, 1931.

[2] Tuplin, W.A., "Dynamic Loads on Gear Teeth", Machine Design, pp. 203, Oct. 1953.

[3] Cloutier J.L. and Tordion G.V., "Dynamic Loads on Precision Spur Gear Teeth According to the Theory of Variable Elasticity". University Laval, Laboratoire d'lements des Machines, Report No. EM-3, June 1962.

[4] Gregory R.W., Harris S.L. and Munro R.G., "Dynamic Behavior of Spur Gears". Proceedings of the Institution of Mechanical Engineers, Vol. 178, No. 8, pp. 261-266, 1963-64.

[5] Cornell, R.W. and Westervelt, J., "Dynamic Tooth Load and Stressing for High Contact Ratio Spur Gears", Journal of Mechanical Design, Vol. 100, No. 1, pp. 69-76, Jan. 1978.

[6] Richardson, H.H.,"Static and Dynamic Load, Stresses, and Deflection Cycles in Spur Gear Systems", Sc. D. thesis, M.I.T. Report, 1958.

[7] Hamad, B.M. and Seireg, A., "Simulation of Whirl Interaction in Pinion-Gear System Supported on Oil Film Bearings,". Journal of Engineering for Power, Transactions of ASME, Vol. 102, pp. 508-510, 1980.

[8] Iida, H., Tamura, A., Kikuchi, K., and Agata, H., "Coupled Torsional-Flexural Vibration of a Shaft in a Geared System of Rotors", Bulletin of Japanese Society of Mechanical Engineers, Vol.23, pp. 2111-2117, 1980.

[9] Iwatsubo, N., Arii, S., and Kawai, R. "Coupled Lateral-Torsional Vibrations of Rotor Systems Trained by Gears (1. Analysis by Transfer Matrix Method)", Bulletin of the Japanese Society of Mechanical Engineers, Vol. 27, pp. 271-277, 1984.

[10] Iwatsubo, N., Arii, S., and Kawai, R. "Coupled Lateral-Torsional Vibrations of Rotor Systems", Proceeding of the Third International Conference on Vibrations in Rotating Machinery (Institution of Mechanical Engineers), pp. 59-66, 1984.

[11] Ozguven, H.N. and Houser, D.R., "Mathematical Models Used in Gear Dynamics". Journal of Sound and Vibration, Vol. 121, No. 3, March 1988.

[12] Ozguven, H. N. and Houser, D. R., "Dynamic Analysis of High Speed Gears by Using Loaded Static Transmission Error", Journal of Sound and Vibration, Vol. 124, No. 2, July 1988.

[13] Lin, H.H.,"Computer-Aided Design and Analysis of Spur Gear Dynamics", Ph.D. Dissertation, University of Cincinnati, 1985.

[14] Lee, C., Lin, H.H., Oswald, F.B., and Townsend, D.P.,"Influence of Linear Profile Modification and Loading Conditions on the Dynamic Tooth Load and Stress of High-Contact-Ratio Spur Gears", ASME Journal of Mechanical Design, Vol. 113, pp. 473-480, Dec. 1991.

[15] Tavakoli, M.S. and Houser, D.R.,"Optimum Profile Modifications for the Minimization of Static Transmission Errors of Spur Gears", ASME Journal of Mechanisms, Transmissions, and Automation in Design, Vol. 107, pp. 529-535, December 1985.

[16] Gargiulo, E.P.,"A Simple Way to Estimate Bearing Stiffness", Machine Design, pp. 107-110, July 1980.

[17] Wang S.M.,"Static and Dynamic Response of Torsional Systems", Ph.D. Dissertation, University of Cincinnati, 1968.

[18] Hahn, W.F.,"Study of Instantaneous Load to Which Gear Teeth are Subjected", Ph.D. Dissertatin, University of Illinois, 1969.

[19] Kasuba, R. and Evans, J.W.,"A Extended Model for Determining Dynamic Load in Spur Gearing", ASME Journal of Mechanical Design, Vol. 103, pp. 398-409, April 1981.

[20] Wang, K.L. and Cheng, H.S.,"A Numerical Solution to the Dynamic Load, Film Thickness, and Surface Temperature in Spur Gears", ASME Journal of Mechanical Design, pp. 177-187, Jan. 1981.

[21] Mark, W.D.,"Gear Noise Origins", Gears and Power Transmission Systems for Helicopters and Turboprops, AGARD CP 369, pp. 30_1-30_14, 1985.

[22] Kubo, A. and Kiyono, S.,"Vibrational Excitation of Cylindrical Involute Gears Due to Tooth Form Error", Bulletin of Japanese Society of Mechanical Engineers, Vol. 23, No. 183, pp. 1536-1543, 1980.

[23] Cornell, R.,"Compliance and Stress Sensitivity of Spur Gear Teeth", ASME Journal of Mechanical Design, Vol. 103, No. 2, pp. 447-459, 1981.

[24] Heywood, R.B.,"Designing by Photoelasticity", Chapman and Hall, Ltd., 1952

[25] Buckingham, E.,"Analytical Mechanics of Gears", Dover Publication, Inc., New York, 1949.

[26] Anderson, N.E. and Loewenthal, S.H.,"Spur Gear System Efficiency at Part and Full Load", NASA TP-1622, 1980.

13. ABSTRACT (Maximum 200 words)

A parametric study of a spur gear system was performed through a numerical analysis approach. This study used the gear dynamic program DANST, a computer simulator, to determine the dynamic behavior of a spur gear system. The analytical results have taken the deflection of shafts and bearings into consideration for static analysis, and the influence of these deflections on gear dynamics was investigated. Damping in the gear system usually is an unknown quantity, but it has an important effect in resonance vibration. Typical values as reported in the literature were used in the present analysis. The dynamic response due to different damping factors was evaluated and compared. The effect of the contact ratio on spur gear dynamic load and dynamic stress was investigated through a parameter study. The contact ratio was varied over the range of 1.26 to 2.46 by adjusting the tooth addendum. Gears with contact ratio near 2.0 were found to have the most favorable dynamic performance.